

Assessing tree root distributions using ground-penetrating radar and machine learning algorithms

John Salako | Neville Millar | Anthony Kendall | Bruno Basso 

Department of Earth and Environmental Sciences, Michigan State University, East Lansing, Michigan, USA

Correspondence

Bruno Basso, Department of Earth and Environmental Sciences, Michigan State University, 288 Farm Lane, East Lansing, MI 48824, USA. Email: basso@msu.edu

Assigned to Associate Editor Phuong Dao.

Funding information

National Institute of Food and Agriculture, Grant/Award Numbers: 2020-67021-32799, 2021-51181-35868; AgBioResearch, Michigan State University

Abstract

Tree cultivation provides food, raw materials, carbon sequestration, and many other ecosystem services. Developing innovative approaches for tree analysis to help optimize their management is crucial. Cherry trees provide numerous health and economic benefits, with Michigan home to 75% of the cherry trees grown in the United States. In this study, we investigated the coarse root architecture of tart cherry trees using non-invasive imaging techniques to reconstruct their spatial distribution and extent. Roots from matured orchards in Michigan were imaged using ground-penetrating radar (GPR) with an 800 MHz antenna. The processed radiograms were analyzed using MALA Vision software, through which a three-dimensional cube was generated. Depth slices extracted from this cube were subsequently analyzed using convolutional neural networks—a novel approach employed to identify and extract root patterns from the imaging data. A nondestructive, controlled root experiment was conducted to validate and assess the detection capabilities of the GPR frequency employed. The findings from this experiment informed the image interpretation process used to reconstruct root geometry. Results indicated that the GPR could detect and reconstruct coarse roots with diameters as small as 4.3 cm. To establish an allometric relationship between root systems and canopy size, an unmanned aerial vehicle was utilized to estimate tree canopy dimensions. Comparative analysis revealed that the lateral extent of coarse roots was approximately 1.2 times larger than the canopy area. Finally, a separate experiment involving root proxies was developed to create a predictive model for root biomass, achieving an accuracy of 95%.

Abbreviations: 3D, three-dimensional; ABR, AgBioResearch Center; AGC, automatic gain correction; AI, artificial intelligence; CNN, convolutional neural networks; EDA, exploratory data analysis; EM, electromagnetic; ERT, electrical resistivity tomography; GPR, ground-penetrating radar; LR, linear regression; MAE, mean absolute error; ML, machine learning; MLP, multilayer perceptron; MSU, Michigan State University; NN, neural network; RBF, radial basis function; RF, random forest; RP, root proxies; RSA, root system architecture; SVM, support vector machine; TC, Traverse City; UAV, unmanned aerial vehicle.

This is an open access article under the terms of the [Creative Commons Attribution-NonCommercial-NoDerivs License](#), which permits use and distribution in any medium, provided the original work is properly cited, the use is non-commercial and no modifications or adaptations are made.

© 2025 The Author(s). *Agrosystems, Geosciences & Environment* published by Wiley Periodicals LLC on behalf of Crop Science Society of America and American Society of Agronomy.

Plain Language Summary

Tree cultivation provides food, raw materials, carbon sequestration, and many other ecosystem services. In this study, we investigated the coarse root architecture of tart cherry trees using non-invasive imaging techniques to reconstruct their spatial distribution and extent. Roots from matured orchards in Michigan were imaged using ground-penetrating radar. We developed a novel approach to identify and extract root patterns from the imaging data. The lateral extent of coarse roots was approximately 1.2 times larger than the canopy area. Finally, a separate experiment involving root proxies was developed to create a predictive model for root biomass, achieving an accuracy of 95%. Our study shows that a suite of non-invasive, integrated, standard, and novel methods can be used to determine tree root distribution and evaluate root weight.

1 | INTRODUCTION

1.1 | Overview

Trees significantly enhance human development and ecological wellness via the ecosystem benefits they provide (Boyd et al., 2013). Trees produce oxygen, absorb carbon dioxide, provide food and shelter, and maintain atmospheric balance via carbon fixation (Baro' et al., 2014; McCarthy et al., 2011).

Trees acquire essential nutrients by absorbing water and minerals from the soil through their roots. Root systems are generally categorized into woody and fine roots (Lantini, Tosti, et al., 2020). The woody roots provide anchorage, while the fine roots extract water and nutrients from the soil and facilitate symbiotic relationships with soil microorganisms (Pregitzer, 2002; Raven et al., 2005). Tree roots' growth and lateral spread vary greatly, influenced by soil types and climates, such as water availability and temperature seasonality (Tumber-D'avila et al., 2022). According to Pallardy (2008), fruit trees grown in sandy soil have roots that laterally spread up to three times the canopy's width, while those grown in loam and clay soils spread twice and one and a half times as far, respectively. We can learn about root diameter, root water content, and distances between roots through root structure analysis (Zhu et al., 2014).

According to Raven et al. (2005), root architecture refers to the spatial configuration and structural organization of a plant's root system within the soil environment. It encompasses root length, diameter, angle, branching pattern, and depth distribution (Lynch, 1995; Gašparíková et al., 2002). Root architecture is a dynamic trait that responds to various environmental and physiological factors, including soil type, moisture availability, nutrient gradients, and plant developmental stage (Hodge, 2004; Smith & De Smet, 2012). Understanding root architecture is critical for assessing plant health, resource acquisition efficiency, and adaptability to environmental stressors (de Dorlodot et al., 2007; Lynch, 2007).

1.2 | Measuring tree root architecture

Understanding root architecture—defined by traits such as root length, diameter, depth, and branching patterns—requires precise and scalable measurement techniques. These techniques generally fall into two categories: destructive and non-destructive. Destructive methods, including root excavation, soil coring, and monolith sampling, allow direct measurement of root traits such as biomass, length, and diameter, and have historically served as ground-truthing standards (Böhm, 1979; van Noordwijk et al., 2004). However, they are labor-intensive and disrupt the soil-root environment, making them less suitable for repeated or large-scale observations.

Non-destructive methods offer alternative ways to infer root architecture without excavation. X-ray computed tomography and magnetic resonance imaging (MRI) enable high-resolution imaging of root systems in controlled environments, capturing traits like root volume and spatial branching (Cui et al., 2011; Tracy et al., 2011). In field settings, ground-penetrating radar (GPR) and electrical resistivity tomography (ERT) have been applied to estimate root biomass distribution, rooting depth, and horizontal spread by detecting contrasts in dielectric and electrical properties between roots and the surrounding soil (Alani & Lantini, 2020; Amato et al., 2009). Specifically, ERT has been widely used in plant-soil studies to detect bulk subsurface heterogeneities by measuring spatial variations in soil electrical resistivity. For instance, Alani and Lantini (2020) demonstrated the utility of ERT in identifying soil compaction zones and monitoring water movement. Similarly, Basso et al. (2010) applied ERT to compare soil resistivity under different tillage treatments. While ERT can indirectly infer zones of high root activity through changes in soil moisture or compaction, it lacks the spatial resolution to detect individual root lengths or other fine-scale architecture.

GPR, by contrast, uses high-frequency electromagnetic (EM) waves to detect dielectric discontinuities between roots

and the surrounding soil, enabling the direct localization of roots under suitable soil conditions. Studies such as Amato et al. (2009) and Zhu et al. (2014) have shown that GPR provides greater spatial resolution for detecting individual roots and estimating root system distribution patterns compared to ERT. GPR has been successfully applied in agricultural and forestry settings to non-destructively quantify root diameter, depth, and lateral spread, making it a valuable tool for high-resolution root architecture analysis when soil conditions permit (Butnor et al., 2001; Guo et al., 2013).

1.2.1 | Ground-penetrating radar

GPR has emerged as a valuable geophysical tool for the non-invasive investigation of subsurface root systems. Initial studies by Hruska et al. (1999) demonstrated GPR's ability to estimate root density and depth in mature oak trees, correlating radar reflections with excavated root structures. Similarly, Daniels (2000) highlighted GPR's potential for estimating root biomass and proposed its application for root carbon quantification in field and laboratory conditions. Subsequent work by Zhu et al. (2014), using an 800 MHz antenna, showed that GPR-based models could estimate root biomass and diameter with relatively low error, detecting coarse roots with a diameter >5 cm and offering a basis for quantifying components of root architecture. Cheng et al. (2014) expanded these insights by testing 250 and 400 MHz antennas to assess their effectiveness in capturing root depth profiles. More recently, Fan et al. (2022) used a 900 MHz antenna to detect roots over 1 cm in diameter and developed an automated three-dimension (3D) root system reconstruction algorithm. The results of their study demonstrated the feasibility and effectiveness of using GPR for root system reconstruction.

While these studies focus on root system reconstruction, it is critical to differentiate this from root architecture, which refers specifically to measurable traits such as total root length, root angle, branching density, and vertical or horizontal distribution (Lynch, 1995). GPR contributes to root architectural analysis by enabling quantification of traits like rooting depth, lateral spread, and coarse root diameter distribution, particularly in conditions where excavation is impractical. The utility of GPR in root architecture studies depends heavily on the careful selection of antenna frequency. Higher frequencies (e.g., ≥ 800 MHz) yield finer resolution required to detect small-diameter roots and finer architectural features, but they are limited to shallow soil depths due to signal attenuation (Millard et al., 2002; Okazaki et al., 2013). In contrast, lower frequencies (e.g., 250–400 MHz) penetrate deeper into the soil but with reduced spatial resolution, making them suitable for detecting larger roots or general depth trends (Jol, 1995).

Core Ideas

- Ground-penetrating radar and convolutional neural network algorithm used for three-dimensional reconstruction of coarse tree roots.
- Machine learning models trained on physical root proxies' traits to predict root weight.
- Unmanned aerial vehicle imagery used for determining tree canopy area and as a potential proxy for root lateral extent.

This trade-off between resolution and depth has significant implications for studying root architecture, as different root traits occur at different spatial scales. For instance, fine root branching and angles may be detectable only with high-frequency signals in the upper soil layers, whereas major roots and deep rooting depth require lower-frequency scans. Consequently, an informed sampling strategy—balancing frequency, scanning depth, and spatial resolution—is essential for capturing the full dimensionality of root architecture.

1.3 | Grid types and tree root measurement

Following the use of the Cartesian grid approach by Hruska et al. (1999), the majority of studies, including those referenced in the previous sections, have followed suit. Based on the literature, the Cartesian grid approach has been mainly used in reconstructing the 3D root geometry and architecture because of its representativeness in assessing root diameter (Fan et al., 2022; Wielopolski et al., 2000; Zhu et al., 2014).

Alternatively, a few researchers have adopted the circular grid pattern in collecting GPR data, an approach favored for easy deployment and the effective detection of root lateral spread and depth. Alani et al. (2018) and Lantini, Giannakis, et al. (2020) used a circular grid approach to study roots with varying GPR antenna frequencies, focusing on tree health assessment and limiting sidewalk damage.

While several studies have explored the application of GPR in root detection and modeling, few have explicitly compared data acquisition strategies based on different scanning geometries, such as grid-based (Cartesian) versus circular sampling schemes. Existing research has demonstrated that circular grids can capture root systems' lateral extent and depth by encompassing the full radial spread around a tree stem (Butnor et al., 2001; Lantini, Tosti, et al., 2020). Although proponents of circular grids often cite their ability to align with the natural radial structure of tree roots (Alani

& Lantini, 2020; Guo et al., 2013), detailed evaluations of their spatial resolution, coverage efficiency, or reconstruction accuracy relative to grid-based methods remain limited in the literature. Therefore, this study contributes to the field by offering a systematic assessment of these acquisition approaches in the context of high-resolution root architecture characterization.

1.4 | Root analysis using artificial intelligence (AI) and neural networks (NNs)

Recent advances in AI, particularly in computer vision and deep learning, are increasingly applied to root system architecture (RSA) analysis. While earlier applications of AI in plant sciences primarily focused on aboveground traits (Hwang & Sugiyama, 2021; S. Li et al., 2023), current approaches now enable automated analysis of complex root traits such as length, area, branching density, and lateral spread through image-based processing techniques (Weihs et al., 2024). Convolutional neural networks (CNNs), in particular, have proven effective in processing 2D and 3D root images for segmentation, feature extraction, and classification (Sordo et al., 2024; Weihs et al., 2024). These methods offer significant accuracy, reproducibility, and scalability advantages, especially for large datasets that would be labor-intensive to analyze manually.

However, most AI applications have focused on visible light or X-ray imagery of root systems, with limited exploration of GPR radiogram data. Integrating AI with GPR—a geophysical method capable of detecting coarse roots—remains an emerging research area. To our knowledge, few published studies have developed or deployed AI models explicitly designed to analyze GPR images for root architectural trait extraction (e.g., root depth, diameter, and spatial distribution; Sun et al., 2023). This gap presents a unique opportunity to advance non-invasive RSA analysis using AI-enhanced GPR interpretation. Our work contributes to this emerging field by applying a CNN model to GPR-derived depth slices to reconstruct RSA (coarse roots) in tart cherry trees.

1.5 | Roots and canopy relationship

Understanding the allometric relationship between canopy size and root system extent can offer valuable insights into tree development and adaptive strategies. This study explores how the lateral spread of tart cherry tree coarse roots relates to canopy dimensions, using GPR to quantify subsurface root extent and unmanned aerial vehicle (UAV) imagery to measure canopy area. Previous research has demonstrated that aboveground structures like canopy width may reflect below-

ground root development patterns (Comas et al., 2005; X. Li et al., 2019), supporting the use of canopy traits as potential proxies for estimating root distribution. By integrating canopy and root data, we aim to establish predictive relationships that may assist in optimizing orchard management practices and improving root zone estimation.

1.6 | Root biomass estimation and relevance to carbon sequestration

Accurately estimating root biomass is essential for understanding plant development and ecosystem carbon dynamics. While destructive methods like excavation and soil coring provide direct measurements, they are labor-intensive and limited in spatial scope (Böhm, 1979; van Noordwijk et al., 2004). As a scalable alternative, researchers have developed models that predict root biomass from above-ground biomass, such as deriving allometric equations from the ratio of shoots to roots. These have proven effective in predicting root biomass and estimating root carbon stock (Mokany et al., 2006).

Moreover, regression and other predictive models have utilized above-ground biomass's geometric features (primarily diameter) to predict or estimate root system biomass (Drexhage & Colin, 2001; Richardson & Zu Dohna, 2003). In this study, we adopt a similar approach by using tree branches, comparable in physical structure to coarse roots, as proxies to develop a predictive model for biomass weight. This supports our GPR-based root detection by linking morphological features to dry biomass.

Root biomass contributes significantly to soil carbon pools through turnover (Jackson et al., 1997). Accurate root measurements inform carbon sequestration quantification (Wielopolski et al., 2000), reinforcing the role of root biomass estimation in ecological and agroforestry research. Carbon content is typically estimated as 50% of the oven-dried biomass weight (Lamlom & Savidge, 2006). Therefore, incorporating machine learning (ML) weight predictive models with accurate root biomass estimation could non-invasively estimate root carbon.

1.7 | Research overview and objectives

The overarching aim of this study is to advance non-invasive methods for quantifying tree RSA using GPR, while exploring the predictive potential of aboveground canopy traits. By integrating field-based geophysical data with remote sensing and ML algorithms, we seek to improve root detection and delineation resolution and accuracy in orchard systems.

To achieve this, the study is guided by the following objectives:

1. Compare two GPR acquisition strategies—Cartesian and circular grids—to assess their effectiveness in reconstructing 3D coarse root architecture and estimating lateral root extent.
2. Utilize high-resolution UAV imagery to quantify canopy dimensions and evaluate its potential as an allometric proxy for lateral root spread.
3. Conduct a controlled buried root-proxy experiment using the same GPR methodology to validate field-based root detection results.
4. Develop an innovative, ML model to predict root weight using known physical characteristics of over one hundred root proxies (RP).
5. Investigate the novel application of artificial NNs to process GPR's reconstructed soil volume depth slices, supporting the reconstruction of coarse root (and root proxy) system architecture.

These objectives contribute to a growing body of research focused on leveraging GPR for high-resolution root mapping and offer practical implications for orchard management and non-invasive root phenotyping.

2 | MATERIALS AND METHODS

This study employed a sequence of integrated field and controlled experiments to evaluate the capacity of GPR to detect and reconstruct the coarse root architecture in tart cherry trees. The experiments were structured to serve complementary objectives. First, two mature tart cherry trees were selected from distinct field locations in Michigan. Each site utilized a different GPR scanning geometry: a Cartesian grid for the Traverse City (TC) tree and a circular grid for the Clarksville AgBioResearch tree. Second, a controlled root proxy experiment was performed to determine the minimum detectable diameter and validate the field experiment of the mature trees under site-specific soil conditions using the Cartesian grid. Third, an ML model was developed to predict biomass weight using dimensional data from 112 shredded tree branches. The ML model was constructed to investigate whether GPR could estimate the weight of the detectable roots. Finally, UAV-based canopy measurements were collected to assess the allometric relationship between root lateral spread and canopy dimensions.

2.1 | Field locations and conditions

Two *Prunus cerasus* (tart cherry) tree fields are as follows (Figure 1b,c, red circles):

1. Bahle field, TC in Leelanau County.

2. Michigan State University (MSU) AgBioResearch Center (ABR), Portland, Clarksville in Ionia County.

TC has sandy loam with an average annual precipitation of 762 mm (Sirrine et al., 2008), ideal for tart cherry growth due to its cold winters and mild summers (Hansen et al., 2018; Ohler, 2023). The ABR site, managed by MSU ABR, features tart cherry trees that are grown in a controlled environment, with further details found on its website. The soil type around the ABR location, according to the USDA Web Soil Survey, is also sandy loam. Michigan provides optimal dormancy and ripening conditions for tart cherries, making the state favorable for cherry production (Me-Nsope, 2009; Vignati et al., 2022).

2.2 | GPR data collection

A MALA ProEx system with an 800 MHz shielded antenna was used for all experiments. Data acquisition parameters were standardized: 2 cm trace separation, 45.45 ns time window, 100 ps sampling interval, and four stacks per trace.

2.2.1 | Cartesian grid (TC site)

At TC, a 5.0×5.0 m Cartesian grid was constructed with 0.15 m line spacing (Figure 2). GPR profiles were collected in perpendicular directions (West-East and South-North) centered around the tree trunk. The grid design was modified near the trunk to accommodate low-hanging branches. This configuration was used in the orchard's 3D tart cherry tree reconstruction. The data were collected by mowing the mounted shielded antenna on a rugged terrain cart.

2.2.2 | Circular grid (Clarksville ABR site)

At ABR, a concentric grid was constructed with radii increasing from 0.65 to 3.25 m in 0.1 m increments (Figure 3). The layout was designed to evaluate root lateral extent more efficiently around the tree's radial spread. GPR data was collected along these circular profiles by moving the shielded antenna with an odometer wheel. A strap affixed around the tree trunk was used to maintain a constant distance (i.e., radius) between the antenna and the trunk. All profiles were collected following a counterclockwise path, beginning from the east side of the trunk.

While the theoretical circumference for each radius ideally defines the profile length, minor discrepancies—typically a few centimeters—were unavoidable due to uneven terrain and the presence of an irrigation system infrastructure. These differences in profile lengths were corrected by recalculating a new trace interval for each profile based on the actual

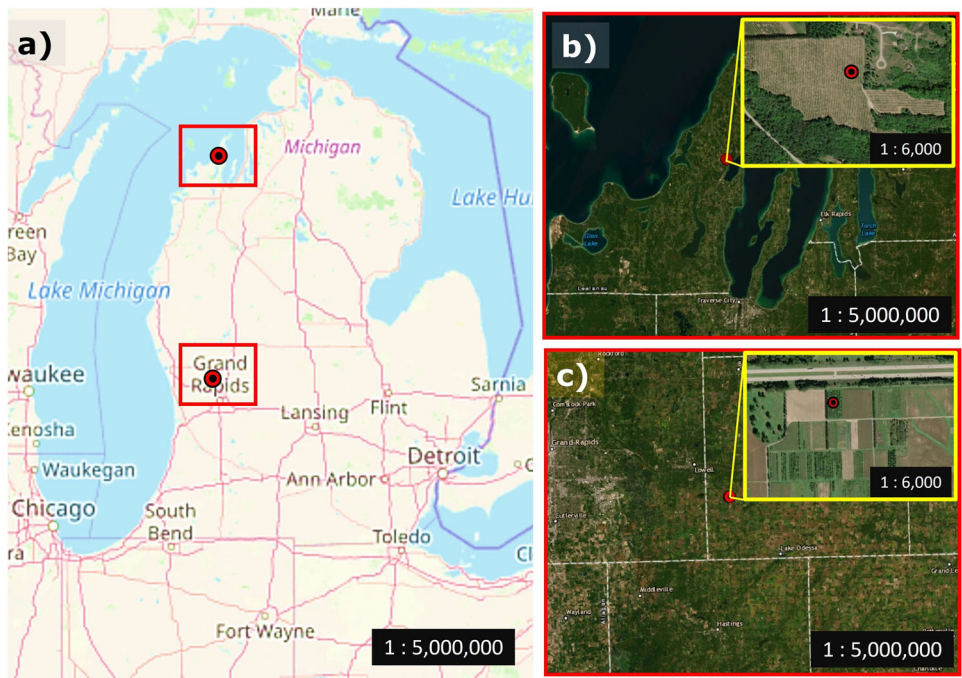


FIGURE 1 Tart cherry tree locations in Michigan. (a) Map of Michigan with marked research sites, (b) a Close-up satellite image of Upper Bahle field located at Traverse City with its surroundings, and (c) a Close-up satellite of the Michigan State University (MSU) AgBioResearch center in Clarksville with its surroundings.

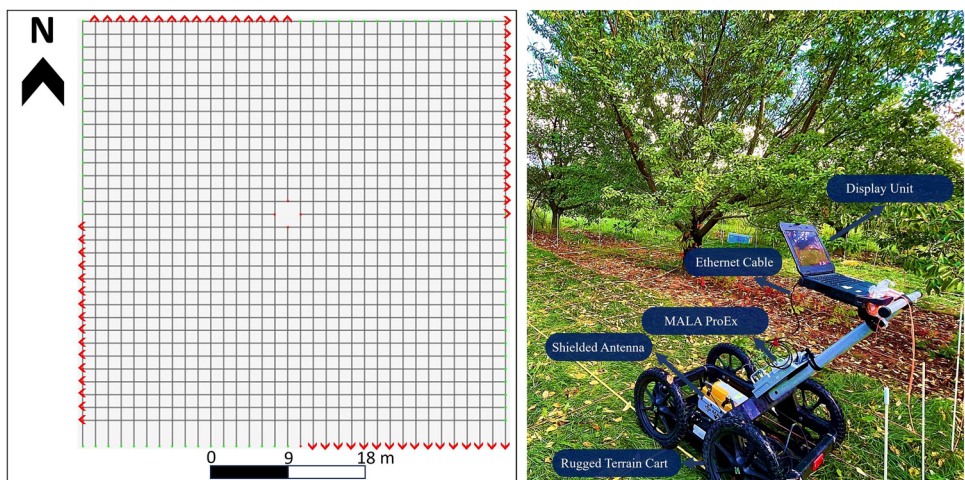


FIGURE 2 Cartesian grid line laid around the tart cherry tree. The right side of the image shows the ground-penetrating radar (GPR) data collection along with the MALA ProEx instrument in front, and the left side of the image shows the reconstructed grid on MALA Vision. The data collection path was influenced by the obstructing stem of the tree.

measured circumference, using the known radius, and applying corrections within ReflexW software (Sandmeier, 2022).

2.3 | Root structure validation via root proxy experiment

A controlled proxy experiment was set up at the MSU Crop and Soil Teaching and Research Center (42.714900,

-84.463300) using a 2.0×2.0 m Cartesian grid. A preliminary experiment using 3- to 5-cm diameter trimmed tree branches was buried at 10- to 30-cm depths. The resulting analysis showed that tree roots <4 cm were not reliably detected; hence, a refined experiment with 4.3–4.9 cm diameter branches was used for the experiment reported in this study (see Figure 4). These trimmed tree branches are called RP and were placed radially to simulate natural branching from a trunk.

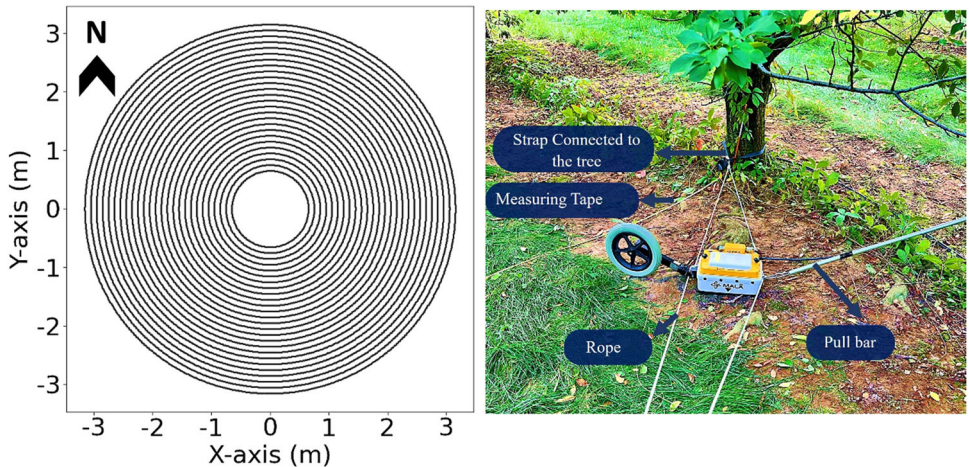


FIGURE 3 Deployment of the circular grid setup around the tart cherry tree. The right side of the image shows the circular grid data instrumentation and collection process, where the measuring tape is laid toward the East, and the antenna is pulled over a counterclockwise route. The left side shows the representation of each circular scan route.

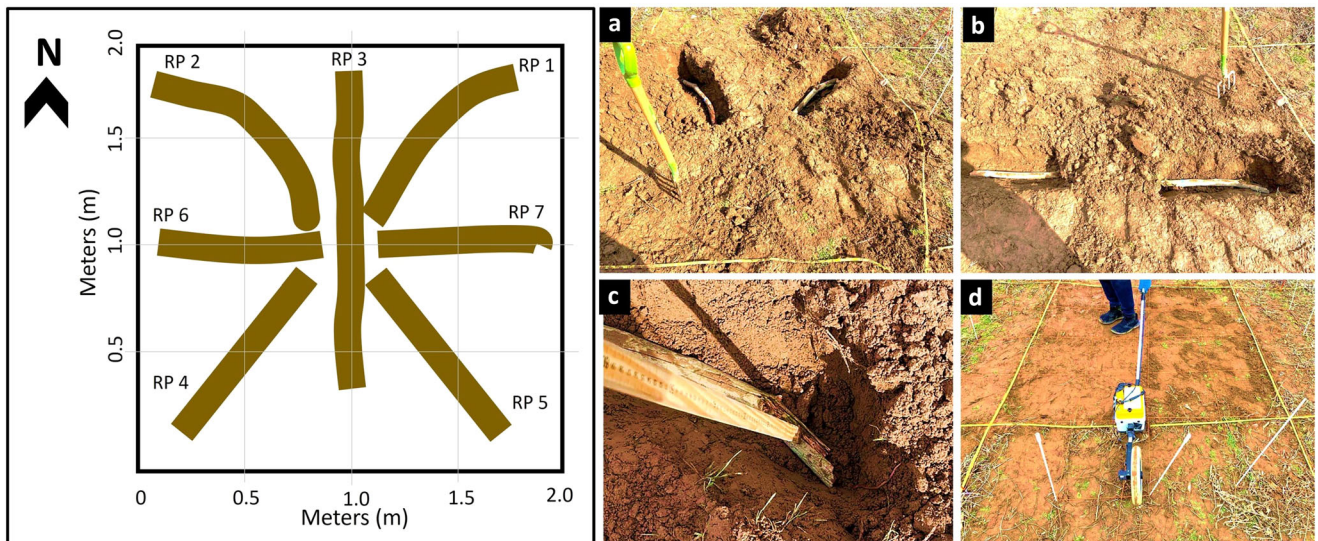


FIGURE 4 Controlled experimental setup. Left-side of the image shows the reconstructed layout of the branches (root proxies [RP]) in the soil with overlaying grid lines of 0.5 m spacing constructed for visual representation. Right-side images show the physical position of the RP in the soil. (a) RP 1 and 2, (b) RP 6 and 7, (c) determining burial depth, and (d) following soil return and compaction to mirror prior undisturbed conditions.

According to Zhang et al. (2019), the main difference between dead and live roots was in their reflection coefficients. Dead roots, characterized by lower water content, exhibited lower reflection coefficients compared to live roots, which contain higher water content. This contrast resulted in poorly developed hyperbolic reflections for dead roots and well-defined hyperbolas in live roots. Building on this knowledge, we were able to utilize the RP to validate the GPR's accuracy in detecting coarse roots from orchards.

Furthermore, we investigated how soil moisture affects the detectability of the RP. Weather and soil moisture data were obtained from the MSU Enviro-Weather station at the

Hancock Turfgrass Center ($42.711000, -84.476000$), located 1.12 km from the experimental site. Before its April 2023 upgrade, soil moisture was measured using vertically installed CS616 sensors (Campbell Scientific) at two depths: 0–30 cm (mstr0) and 30–60 cm (mstr1). After the upgrade, CS650 sensors were installed horizontally at 5, 10, 20, 50, and 100 cm (smst_05 cm to smst_100 cm). Precipitation was recorded with a TE525-L tipping bucket rain gauge, which measures only liquid precipitation (Anon, 2007). Since the maximum burial depth of the RP was 30 cm, we used and reported the minimum and maximum values of mstr0. The soil moisture during the experiment period is categorized as follows:



FIGURE 5 Collected biomass of shredded trees positioned for measurement.

1. *Wet*: $0.31\text{--}0.346 \text{ cm}^3/\text{cm}^3$ (April 4, 2023; few hours after 13.46 mm rainfall)
2. *Moist*: $0.28\text{--}0.30 \text{ cm}^3/\text{cm}^3$ (March 28, 2023; after the previous day's 5.84 mm rainfall)
3. *Dry*: $0.22\text{--}0.23 \text{ cm}^3/\text{cm}^3$ (April 13, 2023); 8 days after last rainfall)

This validation experiment provided an alternative to validating the root detection of the GPR rather than destructively excavating the roots. Also, the soil moisture experiments provided preliminary insight into favorable conditions for GPR-based root imaging under the tested soil type and root proxy setup.

2.4 | Biomass weight prediction model

To support the estimation of root biomass from physical root traits, a predictive model was developed using ML techniques. A total of 112 shredded tree branches (Figure 5)—distinct from the seven buried RP (Figure 4)—were collected to represent a range of sizes. Each sample's physical characteristics, including length, width, and circumference, were measured before drying. The average values of the width and circumference were used in this analysis to account for the RP variability. The biomass samples were oven-dried at 142°F (61°C) for a minimum of 6 weeks until a constant weight was achieved, ensuring moisture loss had stabilized.

The recorded measurements (length, width, and circumference) served as the independent variable for model training. A supervised learning approach was applied to construct the predictive model, which aimed to estimate root biomass weight based on geometric features of the roots. The full experimental workflow and model development pipeline are

documented in Salako (2023), with accompanying codes, datasets, and analysis scripts available in the project's GitHub repository.

2.5 | Root canopy estimation

A Matrice 100 quadcopter (drone) developed by DJI was used to capture the aerial images of the field sites. The drone was outfitted with a visible spectrum red, green, and blue sensor, providing detailed and full-color photographs. The drone's main function was to gather visual data to evaluate the size of tree canopies by capturing aerial images from above the tree line.

Subsequently, the tree canopy images were compared with GPR data of root lateral extent. While the drone images show only the above-ground parts of trees, the size and spread of the tree canopy can be indicative of the root system, as there is often a correlation between the size (diameter) of a tree's canopy and the extent of its roots (Day et al., 2010).

3 | DATA PROCESSING

3.1 | Cartesian grid

The data collected over a square grid (including the controlled experiment) was processed using MALA Vision's 2D window (Guideline Geo, 2023). The processing steps applied to all profiles included:

1. time zero correction,
2. DC Offset correction (Dewow),
3. automatic gain correction (AGC) to compensate for signal attenuation.

Following these processing steps, background removal was performed to eliminate horizontal features and emphasize the diffraction hyperbolae, which are indicative of root structures. This sequence was performed to improve the signal-to-noise ratio in the data and enable more accurate detection of root features.

The soil's EM wave velocity was determined via the hyperbola adaptation method and found to be 0.13 m/ns for the dataset collected around the tart cherry tree in TC. Finally, migration was applied using the same velocity to refocus the scattered energy and sharpen the hyperbolic reflections. The resulting radargram after the 2D processes is shown in Figure 6.

After the 2D processing, all profiles were interpolated to a 3D data cube using the bilinear interpolation function in MALA Vision software (Guideline Geo, 2023). This interpolation allowed for the visualization of root structures in 3D (see

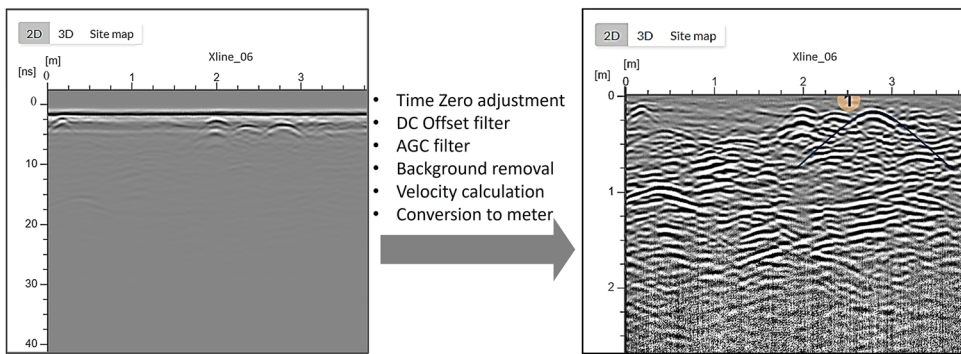


FIGURE 6 The overall processes for a radargram (transect Xline 06) are presented.

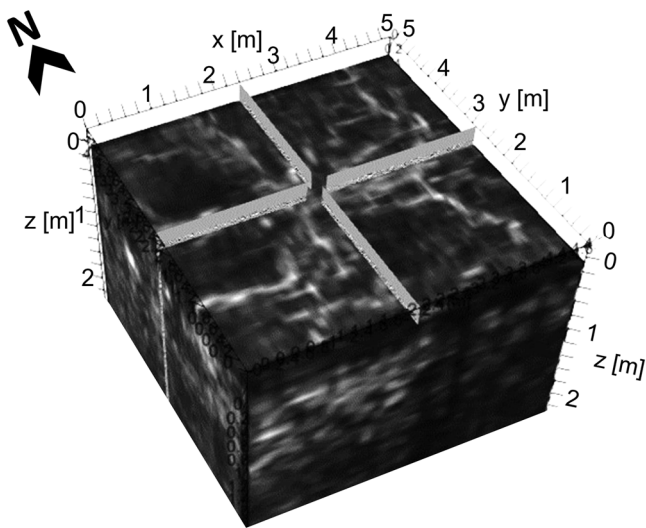


FIGURE 7 Three dimensions (3D) interpolation of the in-lines and cross-lines, showing the roots at a depth of 15 cm.

Figure 7). However, due to residual noise from surrounding soil materials, further processing steps such as segmentation were necessary to isolate and extract the tree roots effectively. We adapted the VGG-16 model for the segmentation processes.

3.1.1 | Transfer learning using VGG16 pre-trained model

We employed a CNN model using the VGG16 architecture with a transfer learning approach to segment root structures from GPR depth slice images. The VGG16 model, developed by Simonyan and Zisserman (2014), consists of 13 convolutional layers with 16 weight layers. We leveraged the first convolutional layer, which contains 64 filters of size 3×3 , to identify root features across the image slices.

Using the TensorFlow library, a simplified model was constructed by extracting and applying pre-trained weights from

VGG16 to the depth slices. Among the 64 convolutional filters, filter 26 yielded the most accurate extraction of root structures and was consistently applied across all depth slices to generate root-only reconstructions.

Further details on the exploratory evaluation of alternate computer vision techniques and model selection rationale are provided in the [Supporting Information](#).

After extracting the roots from the depth slices, ImageJ, an open-source image processing software (Schneider et al., 2012), was used to refine the outputs obtained from the VGG16 model. This refinement involved converting the image into a binary format to emphasize the root structures (Figure 8b), overlaying the binary output onto the original image to compensate for pixel loss during extraction (Figure 8c), and ultimately employing the brush tool in ImageJ to reproduce the root pattern observed in the original root contours (Figure 8d). Subsequently, the processed depth slices were upscaled to the 5×5 m grid dimension and stacked to resemble the original reconstructed soil, reconciling the depth interval between each slice. The ImageJ software generated the 3D volume of the extracted roots using its inbuilt interpolation function.

3.2 | Circular grid

The fixed profile length function in ReflexW (Sandmeier, 2022) was used to revert the trace interval to 0.02 m by resampling the data following the circular GPR profile length correction. A detailed description and formula for this correction are found in Salako (2023).

Following the distance correction, the radargrams were further processed using the same foundational steps applied to Cartesian grid data (see Figure 6), but within the ReflexW software environment, which offers advanced GPR processing functionality. The processing steps included:

1. time zero correction,
2. DC offset correction (Dewow),

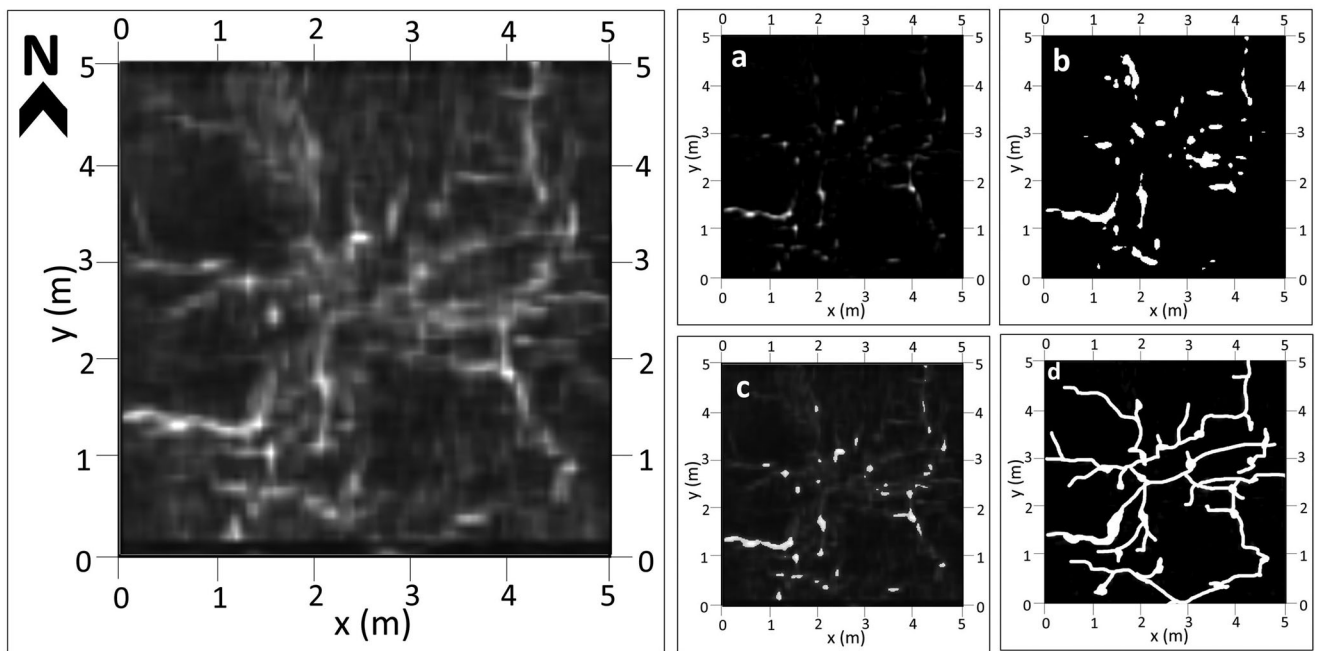


FIGURE 8 The overall image processing of the individual depth slice. The left side of the image shows the screenshot of the depth slice obtained from MALA Vision. The right side shows the image processing steps: (a) root patterns extracted using the VGG16, (b) binary conversion of the image, (c) overlayed original image with the processed image for root pixel correction, and (d) the reconstructed roots image for the depth slice.

3. AGC,
4. application of a Butterworth bandpass filter (300 - 1300 MHz).

A 2D averaging (lowpass) filter was subsequently applied using a 2×2 window (2 samples \times 2 traces) to reduce high-frequency white noise. Background removal was performed to suppress horizontal reflectors and emphasize the diffraction hyperbolae associated with root structures. Finally, frequency-wavelength migration was carried out using a velocity of 0.1 m/ns, determined through hyperbola adaptation.

The fully processed radargrams were exported in ASCII format for post-processing and 3D visualization in Python. Each exported transect represents a 2D amplitude array, with rows corresponding to the horizontal (circular) profile and columns representing signal depth. The recorded depth, originally in nanoseconds, was reconstructed using the acquisition time window (45 ns), and converted to meters using the formula:

$$\text{Depth (m)} = \frac{\text{Time} \times \text{velocity}}{2} \quad (1)$$

where the velocity was 0.1 m/ns, resulting in a maximum depth of 2.25 m. The amplitude values were normalized to a range of -1 to +1 using the MinMaxScaler function from the scikit-learn library (Pedregosa et al., 2011) to prepare the data for further analysis and visualization.

3.2.1 | Reconstruction of the circular transects using Python

To enable visualization in Cartesian space, GPR data collected along circular transects were converted from polar to Cartesian coordinates. This transformation facilitates proper rendering of radargram amplitude values in the x - y plane. The conversion used the following equations:

$$x_i = r \cdot \cos\theta_i \quad (2)$$

$$y_i = r \cdot \sin\theta_i \quad (3)$$

Here, r is the fixed radius of the profile (measured from the tree trunk), and θ_i is the angle associated with the i th trace, derived by dividing the cumulative arc length by the corresponding radius.

An array was created for each transect containing four columns: r , θ , x , and y . The starting radius was calculated as the sum of the tree trunk radius and the distance from the trunk to the initial trace point. As each trace was processed, the x and y values were computed using Equations (2) and (3), and new transects were added by incrementing the radius by 0.1 m, matching the spacing used during data acquisition. This reconstruction produced a 2D representation of the circular grid layout, as shown in the left panel of Figure 3.

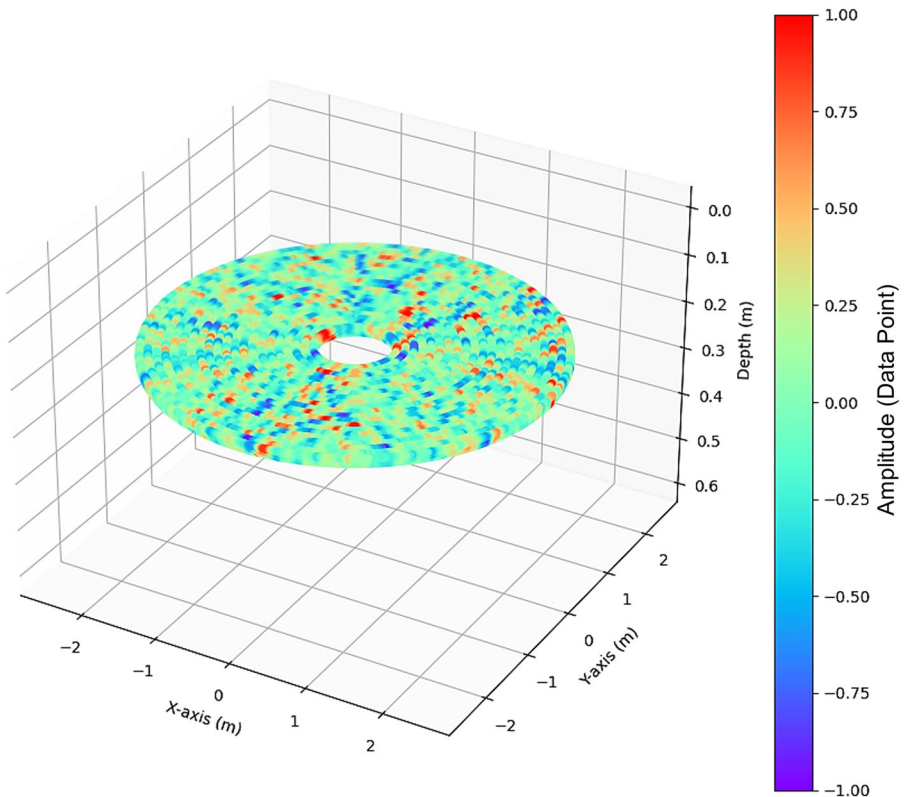


FIGURE 9 Showing the three dimensions (3D) reconstructed depth slice of the uninterpolated scatterplots of the amplitudes at 20-cm depth. The inner and outer diameters are the same throughout the transects, where the inner diameter corresponds to the first transect taken, and the outer diameter corresponds to the last transect taken.

For 3D visualization, depth values associated with each radargram trace were added as the (x_i , y_i , and z_i) for every amplitude point. Using the matplotlib library in Python, each transect was plotted to reconstruct the volumetric space of the soil. This 3D reconstruction allowed individual amplitude values to be spatially located within the cylindrical soil volume surrounding the tree. A mesh was then generated, assigning each amplitude value to its corresponding spatial coordinate. This enabled the construction of 3D depth slices across the circular domain, ultimately producing the root-reflecting image volume shown in Figure 9. The full algorithm implementation for this coordinate transformation, interpolation, and volume rendering is detailed in Section 3 of the Supporting Information.

Slicing through the 3D amplitude volume significantly improves the visual identification of tree roots, as areas of sustained high amplitude typically indicate the presence of root structures. In particular, continuous high-amplitude regions extending outward from the trunk strengthen the interpretation of root distribution patterns.

The amplitude array was sliced horizontally and visualized using the scatter plot function in the Matplotlib library to analyze root spread at specific depths. This allowed for a 2D depth slice representation at chosen depths.

To further enhance visualization quality, Radial Basis Function (RBF) interpolation was implemented using interpolate function from the SciPy library (Virtanen et al., 2020). This interpolation smoothed the discrete amplitude points, producing a more coherent and visually interpretable map of the root system.

Due to the scale of the dataset, comprising millions of amplitude values, interpolation and volumetric rendering were performed on the MSU High-Performance Computing Cluster, maintained by the Institute for Cyber-Enabled Research. This task utilized 10 compute nodes and approximately 500 GB of memory to efficiently process the cylindrical data volume.

3.3 | Buried roots reconstruction

The 2.0×2.0 m Cartesian grid data collected from the buried RP experiment were processed using the same methodology described in Section 3.1. Following radargram processing and interpolation, a 3D soil volume (soil cube) was generated to visualize the buried proxies.

Depth slices extracted from this volume were then analyzed using ImageJ. To quantify the geometric properties of the RP,

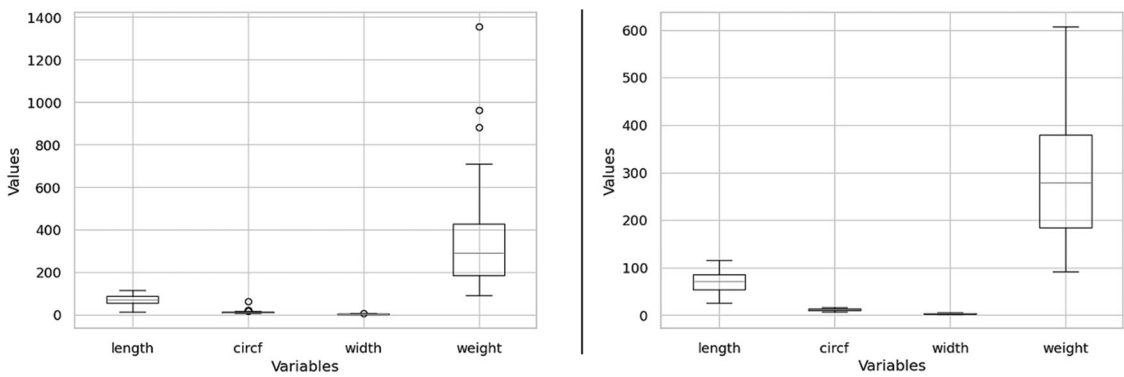


FIGURE 10 Boxplots showing the distribution of root proxy attributes (length, circumference, width, and weight) before (left) and after (right) outlier removal using the IQR method. Outliers are visible in the original data, particularly in the weight and circumference variables. After applying the IQR-based filtering, extreme values were excluded, leading to a more balanced scale for comparative visualization across variables.

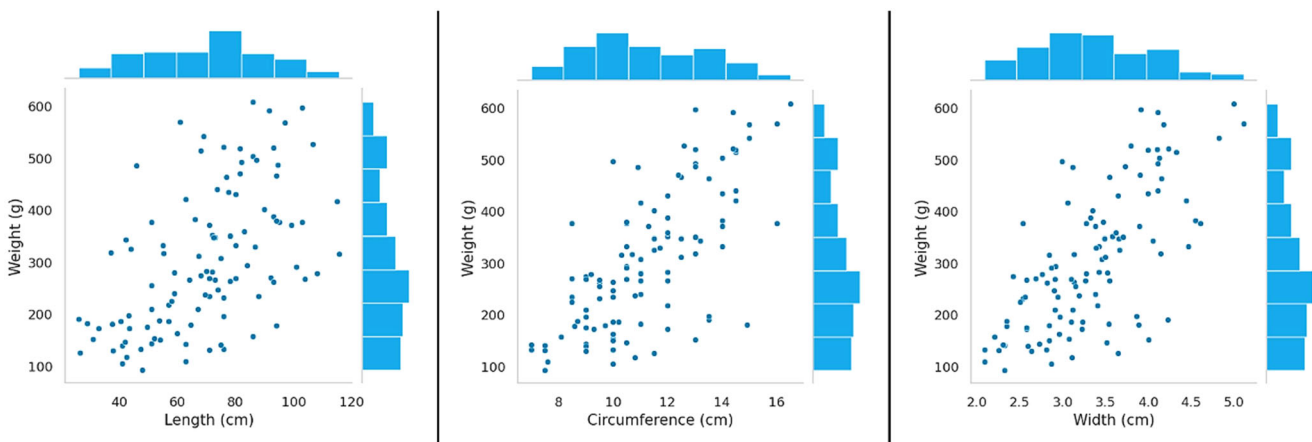


FIGURE 11 Scatter plots with marginal histograms illustrating the relationships between root proxy weight (g) and three physical attributes: length (left), circumference (center), and width (right). All three predictors exhibit positive linear trends with weight, with width and circumference showing the strongest visual correlation. The marginal histograms indicate the distribution of each variable, highlighting relatively normal distributions across the dataset.

the slices were first rescaled to reflect the actual grid dimensions (2.0×2.0 m). The line measuring tool in ImageJ was then used to manually measure the width and length of each visible RP on the selected depth slices. These measurements were used to compare GPR-based root reconstructions against the known physical dimensions of the buried targets, thereby validating detection accuracy.

3.4 | Weight model data processes

Before building the weight model, exploratory data analysis (EDA) was conducted on the collected root proxy dataset. Outliers were detected and removed using the interquartile range (IQR) method, excluding seven entries outside 1.5 times the IQR from the first and third quartiles (see Figure 10). Although formal normality testing was not performed,

the distribution of the geometric variables was approximately symmetric (see Figure 11) and exhibited no severe skewness.

A Pearson correlation analysis was used to assess linear relationships between the independent variables (width, circumference, and length) and the dependent variable (dry weight). All three predictors exhibited strong positive correlations with root weight, with width showing the highest correlation coefficient ($r = 0.71$). Additionally, width and circumference were highly correlated ($r = 0.96$), suggesting that circumference could be inferred from width for buried proxies when direct measurement is not feasible (see Figure 12). Linear regression (LR) models were subsequently fitted using these predictors to estimate root biomass.

Four regression algorithms—LR, support vector machine (SVM), NN, and random forest (RF)—were employed to develop the biomass weight prediction model. After

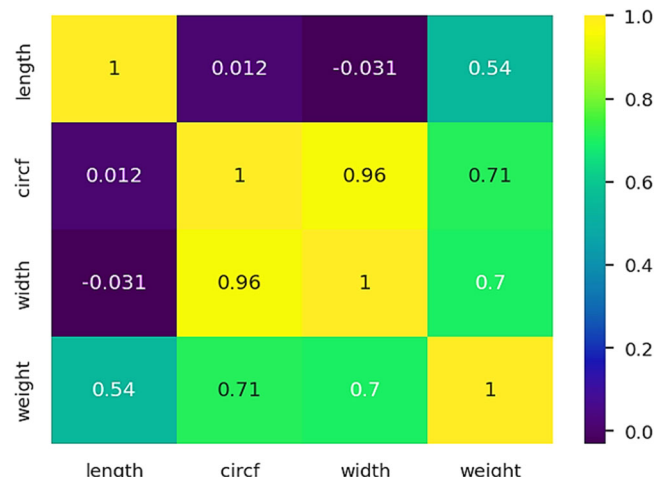


FIGURE 12 Pearson correlation matrix showing pairwise relationships among root proxy variables: length, circumference, width, and weight. Circumference and width exhibit a very strong positive correlation ($r = 0.96$), while both variables are also strongly correlated with weight ($r = 0.71$ and $r = 0.70$, respectively). Length shows a moderate correlation with weight ($r = 0.54$), suggesting it is a less predictive feature in estimating biomass compared to width or circumference.

conducting EDA, the input features were scaled using the MinMaxScaler from the scikit-learn library to ensure uniformity across all models. The dataset was then randomly split into 80% for training and 20% for testing. Model performance was evaluated using fivefold cross-validation, where the dataset was partitioned into five random subsets.

All regression models were implemented using scikit-learn (Pedregosa et al., 2011). Grid search was used to find the optimal parameters, and the following hyperparameters were set:

- LR: Used with default parameters.
- SVM: Implemented using SVR (kernel = “RBF”, $C = 100$, gamma = 0.01, epsilon = 0.3) to account for non-linearity in the input-output relationship.
- NN: Built using MLPRegressor(hidden_layer_sizes = (2000,), activation = “relu”, solver = “adam”, max_iter = 40, random_state = 42, learning_rate_init = 0.001) for single hidden layer regression with adaptive moment estimation.
- RF: Configured with RandomForestRegressor(n_estimators = 6, max_features = 2, random_state = 42) to ensure sufficient ensemble learning without overfitting.

Model accuracy was assessed using mean absolute error (MAE) as the evaluation metric (Schneider & Xhafa, 2022). For theoretical foundation and implementation, see Aurelien (2017).

3.5 | Canopy image processing

After collecting and processing the UAV imagery from the Matrice 100 quadcopter, the canopy images were orthomosaicked (stitched) and imported into ArcMap (<https://digitalcommons.usu.edu/cgi/viewcontent.cgi?article=2917&context=extension%5Fcurlallsri>, 2011) for analysis. Using the measurement tool, the canopy geometry of the sampled mature tart cherry trees at the ABR and TC sites was quantified. Specifically, the canopy length (North-South direction), canopy width (West-East direction), and projected canopy area were measured, as illustrated in Figure 13. These canopy metrics were subsequently compared to the spatial extent of the subsurface coarse root structure obtained from GPR data, enabling the evaluation of aboveground-belowground spatial relationships (see Section 4.3).

4 | RESULTS

4.1 | Cartesian grid

Using the Cartesian grid method, the processed time slices were stacked and interpolated to generate a 3D volume of the subsurface root system. The final reconstruction revealed multiple high-amplitude reflections radiating outward from the tree trunk, indicating the presence of large lateral roots. Roots were consistently detected between depths of 10 and 50 cm, with the most prominent reflections concentrated in the upper 30 cm of the soil profile. The reconstructed volume, shown in Figure 14, confirms a symmetrical root spread extending up to approximately 2.5 m from the trunk in all directions, matching the predefined 5×5 m scan area.

4.2 | Circular grid

The circular grid reconstruction for the ABR tree also revealed distinct high-amplitude reflections indicative of root presence. Roots were observed at depths ranging from 10 to 45 cm, with the most continuous and pronounced reflections located between 15 and 35 cm. Lateral root extension was evident across the radial profiles, with high-amplitude signals present up to the final transect at a radius of 3.2 m, corresponding to a total lateral spread (diameter) of approximately 6.4 m. These results, shown in Figure 15, suggest a well-developed and symmetrical root system, consistent with mature tree morphology.

4.3 | Canopy and root comparison

In the case of the TC tree (Cartesian grid), the canopy dimensions determined from ArcGIS functionality showed a

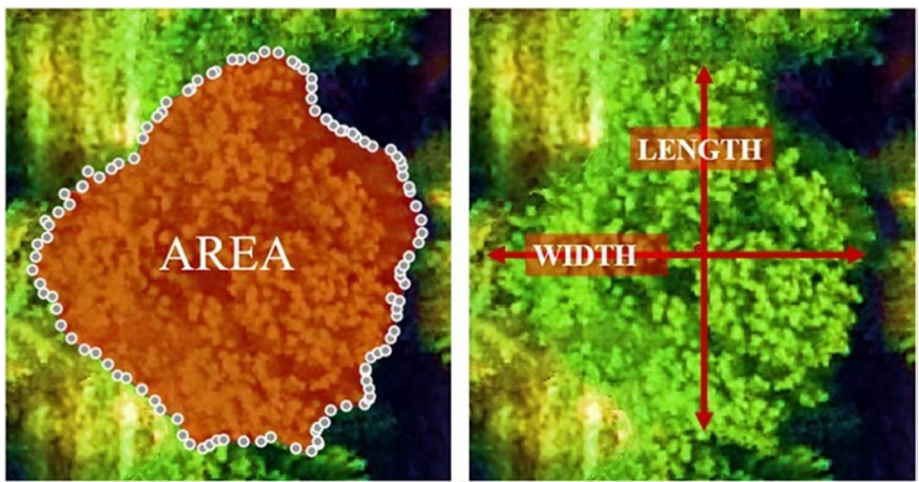


FIGURE 13 Showing the method employed to determine the canopy size using ArcGIS's measurement tool.

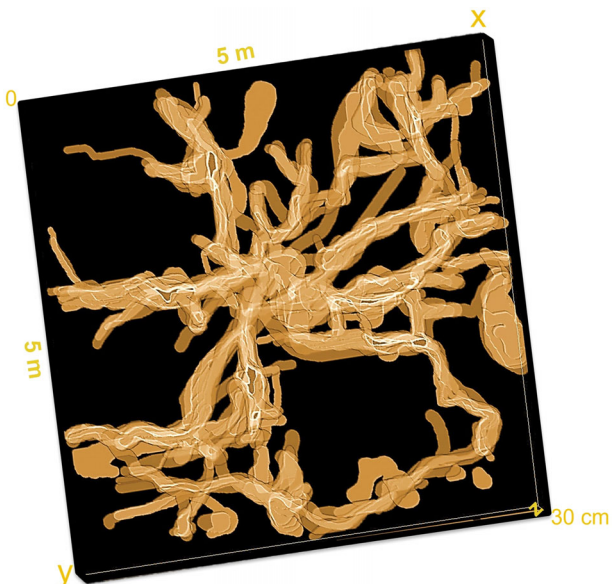


FIGURE 14 Three dimensions (3D) reconstructed roots of the Traverse City (TC) tree, spatially distributed in the 5×5 m grid.

maximum length of 5.39 m and a maximum width of 4.18 m. The area of the canopy was measured using the polygon area function in ArcGIS and was measured as 20.41 m^2 . The root distribution appeared mostly contained within the 5.0×5.0 m sampling area (25.0 m^2); however, some reflections extended toward the grid edge, suggesting the roots may spread further beyond the scanned region. We constrain our results based on the collected data and report the coarse root area as 5.0×5.0 m (25.0 m^2), with a resulting measured root-to-canopy area ratio of 1.22.

For the ABR tree (circular grid), the canopy polygon had maximum dimensions of 6.73 m (length) \times 6.84 m (width), with a measured polygon area of 32.99 m^2 . The radial root extent, based on outermost high-amplitude reflections (radius

≈ 3.2 m), formed a circular root polygon with an area of 32.17 m^2 . Although some roots likely extended beyond the radius surveyed, we constrain the results based on the data collected. The lateral extent of the reconstructed coarse roots was observed at 6.4×6.4 m, covering an area of 40.96 m^2 , resulting in a root-to-canopy area ratio of 1.24. The dimensions (width, length, area) for the canopy, root area, and the root-to-canopy area for the ABR and TC trees are summarized in Table 2. Figure 16 overlays these canopy and root polygons for spatial comparison.

It is important to note that both root areas represent GPR-interpreted lateral spread and are limited by survey boundaries and antenna frequency, which may not capture finer roots or deeper structures.

4.4 | Root weight model evaluation

The MAE values for each model from the fivefold cross-validation are presented in Table 3. Among the regressors, SVM and RF regressors achieved the lowest MAEs, outperforming the multilayer perceptron (MLP) and LR models across the five data subsets (Table 3).

The best-performing test model was obtained using a random seed value of 5 (seed = 5). Seed values were used to ensure consistent and reproducible data splits, cross-validation folds, and model initialization. Under this setting (seed = 5), the test results showed percentage prediction errors of 5.08% (RF), 8.27% (SVM), 10.79% (LR), and 11.30% (MLP).

As illustrated in Figure 17, the predicted weights are plotted against the measured weights using scatter plots. The solid diagonal line represents a perfect match between predicted and measured values. The RF and SVM regressors showed strong alignment with the actual data, confirming their superior predictive performance in this study.

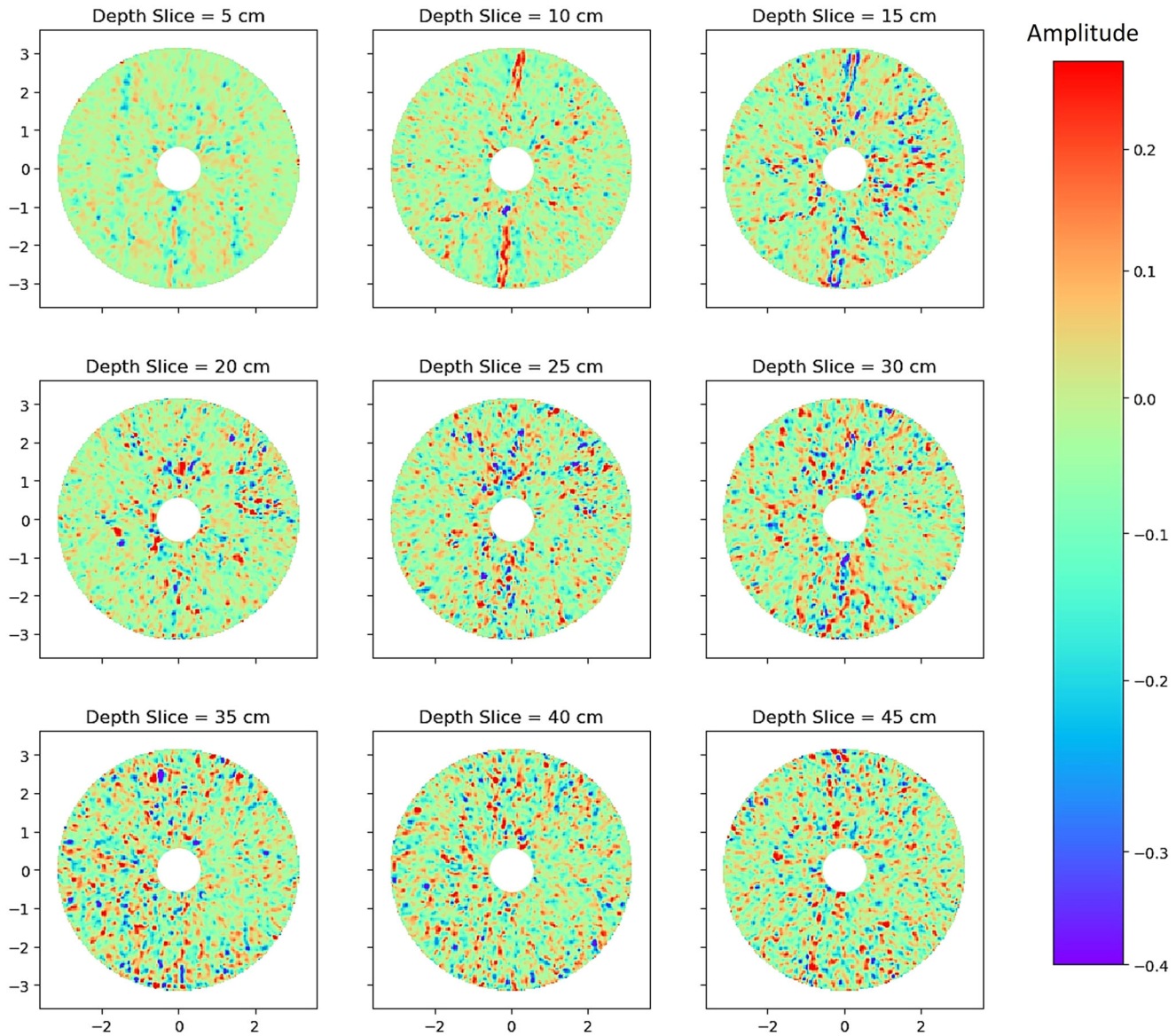


FIGURE 15 Interpolated results of the depth slices for the AgBioResearch Center (ABR) tree, spanning from 5- to 45-cm depth. The higher amplitudes (red color) in the plots correspond to the root of the trees, as they extend from the center of the tree's trunk.

4.5 | Controlled experiment

The reconstructed biomass geometry and position, as shown in Figure 18, exhibited strong alignment with the actual buried RP locations. The GPR-estimated depths of the proxies deviated by an average of ± 3 cm from their known burial depths.

Figure 18a shows the overall agreement between the reconstructed RP layout and the known burial map (Figure 4). In Figure 18b, the 3D depth slice 13 corresponds to RP 1, RP 4, RP 5, RP 6, and RP 7, which were buried at approximately 20 cm.

The small depth errors and spatial alignment between GPR-derived and actual RP positions provide empirical support for the model's reconstruction accuracy.

5 | DISCUSSION

5.1 | Cartesian grid analysis and root diameter detection

The roots of the TC tart cherry tree spread out in a lateral direction to cover our sampling area (5×5 m), likely extending even further, going as deep as 0.3 m. The smallest continuous root that we could measure had a diameter of 4.3 cm and was consistent with our expectations of the capability of the 800 MHz antenna based on previous studies. For instance, Zhu et al. (2014), using an 800 MHz antenna frequency, detected coarse roots with a diameter >5 cm, while Fan et al. (2022) were able to detect roots >1 cm using a 900 MHz antenna frequency. Molon et al. (2017) used a 1 GHz

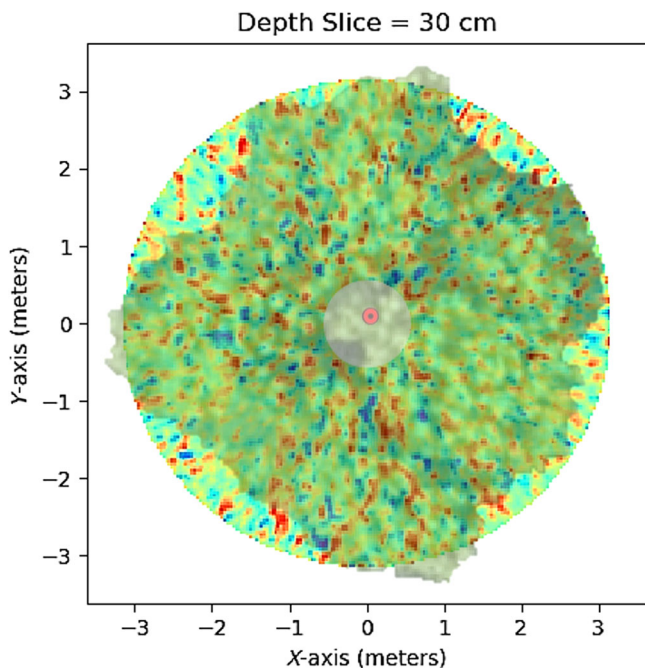


FIGURE 16 Overlay of the reconstructed root distribution and canopy extent of the AgBioResearch Center (ABR) tree at a depth slice of 30 cm. The red dot marks the tree trunk position, georeferenced during field data collection. The circular root distribution is derived from high-amplitude ground-penetrating radar (GPR) reflections, while the shaded canopy polygon represents the crown extent extracted from unmanned aerial vehicle (UAV) imagery. Although the visible canopy extends beyond the scanned root area, the actual root system likely exceeds the scanned extent.

frequency to detect coarse roots >1.4 cm, and Bain et al. (2017) were able to detect coarse roots of 0.5 cm in diameter using a 1.5 GHz antenna frequency.

From literature and as defined in Zhang and Wang (2015), coarse roots are roots with a diameter ≥ 0.2 cm, and fine roots are defined with a root diameter <0.2 cm. Consequently, higher antenna frequencies could potentially detect fine roots in the soil, as there are GPR frequencies that scale up to 2.3 GHz (MALA PROEX SYSTEM). However, signal attenuation at this frequency would likely limit its use to very shallow investigations (Jol, 2008).

In addition to the antenna frequency, clay and soil moisture significantly impact the penetration depth and object size detection capabilities of GPR. Clay soils are highly conductive, causing attenuation of the GPR frequency and resulting in a shallower depth of penetration (Chanzy et al., 1996; Tosti et al., 2013). Similarly, soil moisture content reduces the penetration depth of the GPR frequency. Wet soil conditions, especially in conductive soils such as clay, can further reduce the penetration depth of the radar signal. This is because moist soils, having higher electrical conductivity, cause more absorption and scattering of the radar waves (Lunt et al., 2005; Zajícová & Chuman, 2019). As a result, using the same GPR

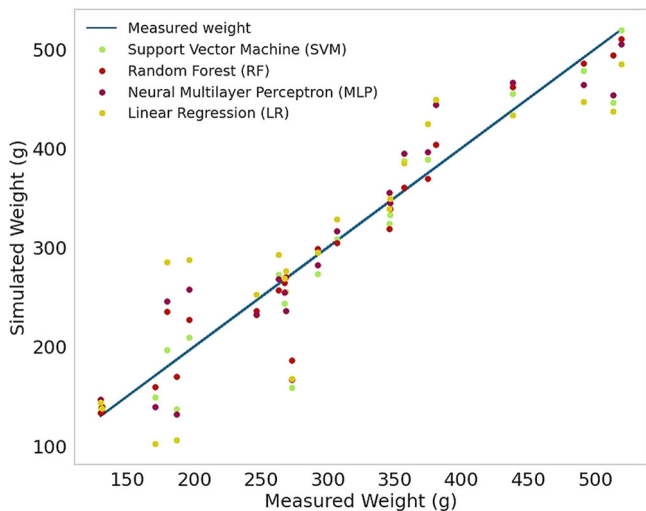


FIGURE 17 Comparison of predicted and measured biomass weights (g) for the test dataset (seed = 5) using four regression models: support vector machine (SVM), random forest (RF), multilayer perceptron (MLP), and linear regression (LR). The solid blue line represents the 1:1 reference line, indicating perfect agreement between predicted and measured values. Data points are color-coded by regression model. While the predicted values for RF and SVM closely follow the 1:1 line, indicating strong model performance, further evaluation metrics.

frequency can produce different penetration results and object detection depending on the nature of the soil.

To gain insight into the most favorable moisture conditions for root detection in sandy-loam soil, data from the controlled experiment were collected under three soil conditions (“wet,” “moist,” and “dry,” Section 2.2.2). Detailed analyses of these results, including images of soil conditions, are in Salako (2023). As stated in Section 2.3, Zhang et al. (2019) investigated GPR’s sensitivity in detecting live roots and dead roots (branches as RP). They concluded that the main difference between the two types of roots was in the definition of the hyperbolas, but both roots were detected by the GPR, which supports the viability of our approach. We used trimmed branches as RP to evaluate GPR accuracy in detecting roots under these soil conditions, and the results are presented here. The findings showed that GPR can effectively detect biomass (RP) when there is a clear contrast between the RP and soil. The distinction of RP from the soil matrix was most apparent in the “moist” soil, where all RPs could be effectively distinguished. Under “dry” soil conditions, GPR successfully identified the geometry of one root proxy (RP 1) with high accuracy. However, it failed to recognize the other RP, possibly due to the superficial dryness of the soil beneath the surface. Under “wet” soil conditions (after 13.5 mm of rainfall), GPR’s performance was further hampered; the roots became indistinguishable from the soil.

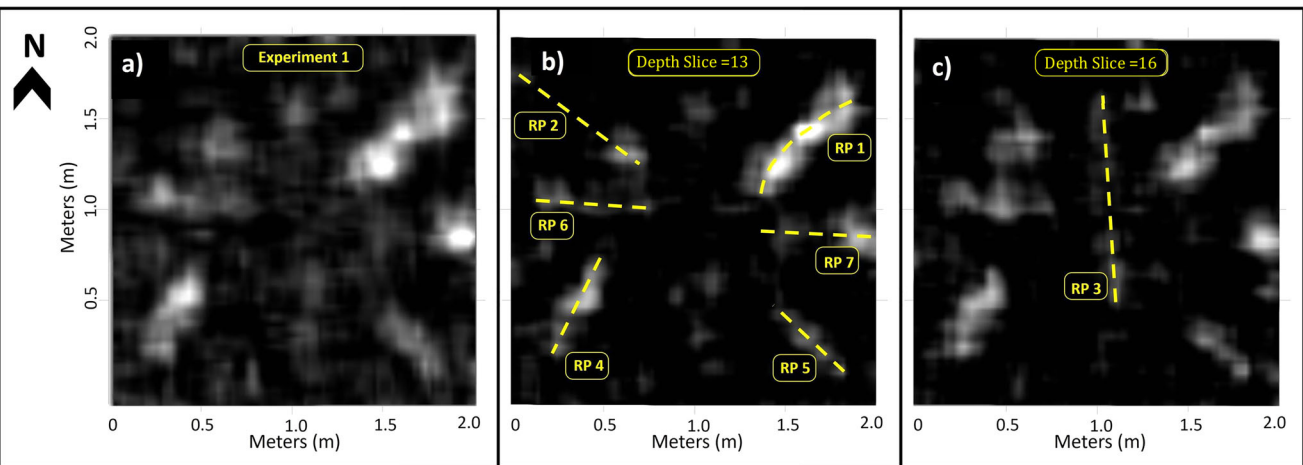


FIGURE 18 Left to right image showing the processed buried root proxies (RP) and showing the different depths correlating with where the roots were buried. The images also highlight the visual alignment with the actual buried positions as seen in Figure 4. Subfigure (a) shows the overall reconstructed roots, and Subfigures (b) and (c) show the measurement of the RP.

TABLE 1 Branch (root proxy) identification and measurements prior to burial.

Root proxy (No.)	Length (cm)	Width (cm)	Circumference (cm)	Depth (cm)
RP 1	84	4.90	16.5	16–20
RP 2	97	4.30	14.0	10–15
RP 3	104	4.55	15.5	20–30
RP 4	51	4.30	15.0	15–24
RP 5	56	4.86	16.5	22–25
RP 6	64	4.33	14.0	17–20
RP 7	68	4.80	16.0	17–20

Abbreviation: RP, root proxies.

TABLE 2 Summary table of the measured canopy and root area comparison.

Tree site	Canopy length (m)	Canopy width (m)	Canopy area (m ²)	Root area (m ²)*	Root-to-canopy area ratio
TC (cartesian)	5.39	4.18	20.41	25.00	1.22
ABR (circular)	6.73	6.84	32.99	40.96	1.24

Abbreviations: ABR, AgBioResearch Center; TC, Traverse City.

Although our experiment did not include overlapping RP, we ensured that the RP were buried at different depths, as shown in Table 1 and Figure 4. The results showed an average error of ± 3 cm between the burial depth and the reconstructed depth. Additionally, as shown in Figures 18b,c, the GPR time slices visually match the physical structure of the RP in Figure 4, allowing for a direct comparison of the reconstructed root geometry with the original RP geometry. These findings indicate that, for an 800 MHz antenna frequency, roots of at least 4 cm can be detected and distinguished by the GPR.

Our results are corroborated in the literature by Butnor et al. (2001, 2005), who showed that increasing soil moisture

content increases signal attenuation and complicates the distinction between live roots and buried organic matter. Their research showed that roots would be indiscernible when the soil moisture content around the roots was made to equalize with the root moisture content. The relative dielectric permittivity (ϵ_r) of the soil and the roots may provide further explanation. Wet sandy-loamy soil has an average ϵ_r value of 22.5, while dry wood cellulose has a ϵ_r value of 4.5, in contrast to wet wood cellulose, which has a ϵ_r value of 22 (similar to the wet sandy-loamy soil) (Attia al Hagrey, 2007). The ability of the GPR to reflect signals is largely dependent on the difference in ϵ_r values between the object (root) and the surrounding medium (soil), making moisture content in the roots

TABLE 3 Model evaluation showing the five models' mean absolute error (MAE) and the percentage error (%).

Test models (seed)	SVM MAE (%)	RF MAE (%)	MLP MAE (%)	LR MAE (%)
20	25.69 (11.95)	24.62 (9.54)	32.92 (14.37)	38.67 (15.76)
300	28.08 (11.60)	20.97 (10.92)	31.36 (13.54)	41.31 (14.89)
2	35.73 (14.98)	23.68 (10.46)	36.69 (14.53)	43.96 (17.24)
100	37.75 (11.65)	26.51 (4.77)	39.05 (12.75)	38.90 (16.23)
5	19.27 (8.27)	12.48 (5.08)	24.93 (11.30)	26.40 (10.79)
Average	33.75 (11.69)	25.77 (8.15)	35.44 (13.29)	39.27 (14.98)

Note: The seed here is the random generator used for the data points selection.

Abbreviations: LR, linear regression; MLP, multilayer perceptron; RF, random forest; SVM, support vector machine.

and in the soil a critical factor (Attia al Hagrey, 2007; Guo et al., 2013).

Work by Guo et al. (2013) suggests that optimal conditions for successful GPR root detection are found in well-drained, electrically resistive soils, such as sand, particularly under dry conditions. These conditions were typical of the TC tree location (Cartesian grid) in summer, characterized by rich, sandy soil, resulting in a sharp contrast between the roots and the soil (Figure 8).

5.2 | Relationship between the canopy and the roots' spatial distribution

Root diameter is typically reduced as it extends outward laterally (Danjon & Reubens, 2008; Fan et al., 2022). This and our inability using the 800 MHz antenna frequency to detect root diameters <4.3 cm (see controlled experiment) indicate a high likelihood that our studied roots extended beyond the measured areas of 25 m^2 and 40.96 m^2 for the TC tree and ABR tree, respectively. Our ratio results are corroborated by Sinacore et al. (2017) and Tumber-Da'vila et al. (2022), who found that total root lateral extent was at least 1.25 and 2.2 times that of canopy extent, respectively. In fruit trees, Pallardy (2008) also found that fruit tree roots could extend three times wider than the canopy.

5.3 | Weight model analysis

Our results demonstrate the potential to develop a generalizable, predictive tree root weight model. Using the width, circumference, and length of 112 tree branches (RP), we built ML models, the best of which showed a 5% overall weight error when compared to the actual biomass weight. The addition of a root density metric, recognizing that it varies (Dias et al., 2018; Kimberley et al., 2015; MacFarlane, 2020), to the ML models could further improve their prediction accuracy. Representative weight models could also yield a realistic estimate of tree roots and overall tree biomass carbon. Root

weight can be converted to root carbon content by conversion factors, for example, 0.5 g C/g (Kurz et al., 2009; Morhart et al., 2016; Pretzsch, 2009). An increasingly vital ecosystem service of trees is their role in carbon sequestration in the soil, especially through their expansive root systems (Oelbermann et al., 2004). The need to sequester carbon is important to offset carbon dioxide emissions and mitigate climate change (Domke et al., 2020; Mildrexler et al., 2020). Root-sourced carbon is more preserved in the soil than aboveground carbon fixed in biomass due to its physical and chemical interactions with the soil (Lorenz & Lal, 2014).

We proposed to use the reconstructed length, width, and circumference of the buried RP to estimate the known weight of the biomass. However, although the reconstructed root length was in good agreement with the measured length (errors from -19.12% to 9.52%), the reconstructed width measurements in 2D had a higher error (Figure 18). This issue may be linked to the method of grid interpolation used for analysis. Under "moist" soil conditions, GPR data were collected immediately after biomass burial, and despite efforts to ensure close contact between the biomass and soil through compacting the soil (foot pressure applied), there were likely gaps between the biomass and soil matrix, which led to errors in width estimation. In contrast, under "dry" conditions, which were assessed several days following rainfall, RP 1 was accurately reconstructed. It is likely that the intervening rainfall and dry period allowed for the soil "settling" around the biomass, improving the contact and, consequently, the GPR detection accuracy.

To help ameliorate this issue, future work should include manual watering of the soil surrounding the buried biomass and allowing the soil to dry over several days while conducting GPR measurements during that time. This could provide more reliable and systematic information on the conditions under which GPR "works" with improved resolution and more accurate width estimates of buried biomass.

Although the weight estimation model could not be effectively validated, the minimal testing error (5%) of the trained weight estimation model demonstrates the potential of using ML models to estimate tree root weight to be incorporated into root biomass models. We expect the model accuracy to

increase, given more training data and the addition of the density metric variable.

6 | CONCLUSION

Combining GPR with AI tools, particularly ML, is a promising approach for studying tree roots. With GPR, AI, and complementary Cartesian and circular grid approaches, we successfully generated images of the root architecture and root extent of mature orchard cherry trees.

The use of high GPR antenna frequency (≥ 2.0 GHz) and further root proxy experiments on controlled soil moisture gradients will allow for the detection of smaller-diameter tree roots and provide more information on environmental conditions where the method can be successfully deployed.

The use of UAVs to indirectly determine (via canopy area) tree lateral root extent is promising but, alongside root GPR studies, requires more testing on a greater variety of trees throughout their growing period.

ML models to estimate tree biomass show potential. Their accuracy will be improved with more training data and the inclusion of root density metrics.

Integrating remote sensing (UAV) tree canopy data with root biomass models can help improve estimates of orchard and agroforestry productivity that, in turn, will better inform options for management practices. Biogeochemical models of these systems will also benefit with improved accuracy in the estimation of their (root) carbon content and flow.

AUTHOR CONTRIBUTIONS

John Salako: Data curation; formal analysis; methodology; software; validation; visualization; writing—original draft; writing—review and editing. **Neville Millar:** Writing—original draft; writing—review and editing. **Anthony Kendall:** Methodology; writing—review and editing. **Bruno Basso:** Conceptualization; funding acquisition; project administration; resources; supervision; validation; writing—review and editing.

ACKNOWLEDGMENT

The authors would like to express their sincere gratitude to Dr. Mine Dogan for her valuable comments on the manuscripts, Dr. Michael Murillo for his support in the image analysis, and Chanho Park, Nazife Onaral, Aylin Yildirim, and the Basso Lab members for their help in the data collection. Funding for this work was provided by USDA SCRI Cheery Project, USDA NIFA, AIFARM Award no. 2020-67021-32799, Michigan State University, AgBioResearch.

CONFLICT OF INTEREST STATEMENT

The authors declare no conflicts of interest.

DATA AVAILABILITY STATEMENT

The processed GPR data collected for the trees, weight model, source codes, and Jupyter Notebook analysis files for this study are publicly available on the GitHub page (<https://github.com/TheGospeler/Root-Distribution-Analysis-and-Computation/tree/main>)

ORCID

Bruno Basso  <https://orcid.org/0000-0003-2090-4616>

REFERENCES

- Alani, A., Ciampoli, L. B., Lantini, L., Tosti, F., & Benedetto, A. (2018). Mapping the root system of matured trees using ground penetrating radar. In *2018 17th International Conference on Ground Penetrating Radar (GPR)* (pp. 1–6). IEEE. <https://doi.org/10.1109/ICGPR.2018.8441535>
- Alani, A. M., & Lantini, L. (2020). Recent advances in tree root mapping and assessment using non-destructive testing methods: A focus on ground penetrating radar. *Surveys in Geophysics*, *41*, 605–646. <https://doi.org/10.1007/s10712-019-09548-6>
- Amato, M., Bitella, G., Rossi, R., Gómez, J. A., Lovelli, S., & Gomes, J. J. F. (2009). Multi-electrode 3D resistivity imaging of alfalfa root zone. *European Journal of Agronomy*, *31*(4), 213–222. <https://doi.org/10.1016/j.eja.2009.08.005>
- Anon. (2007). *MSU Enviroweather*. Data on Demand. <https://mawn.geo.msu.edu/>
- Attia al Hagrey, S. (2007). Geophysical imaging of root-zone, trunk, and moisture heterogeneity. *Journal of Experimental Botany*, *58*(4), 839–854. <https://doi.org/10.1093/jxb/erl237>
- Aurelien, G. (2017). *Hands-on machine learning with scikit-learn & tensorflow*. Shroff/O'Reilly.
- Bain, J. C., Day, F. P., & Butnor, J. R. (2017). Experimental evaluation of several key factors affecting root biomass estimation by 1500 MHz ground-penetrating radar. *Remote Sensing*, *9*(12), 1337. <https://doi.org/10.3390/rs9121337>
- Baro', F., Chaparro, L., Gómez-Baggethun, E., Langemeyer, J., Nowak, D. J., & Terradas, J. (2014). Contribution of ecosystem services to air quality and climate change mitigation policies: The case of urban forests in Barcelona, Spain. *Ambio*, *43*, 466–479. <https://doi.org/10.1007/s13280-014-0507-x>
- Basso, B., Amato, M., Bitella, G., Rossi, R., Kravchenko, A., Sartori, L., Carvahlo, L. M., & Gomes, J. (2010). Two-dimensional spatial and temporal variation of soil physical properties in tillage systems using electrical resistivity tomography. *Agronomy Journal*, *102*(2), 440–449. <https://doi.org/10.2134/agronj2009.0298>
- Böhm, W. (1979). *Methods of studying root systems*. Springer. <https://doi.org/10.1007/978-3-642-67282-8>
- Boyd, I., Freer-Smith, P., Gilligan, C., & Godfray, H. (2013). The consequence of tree pests and diseases for ecosystem services. *Science*, *342*(6160), 1235773. <https://doi.org/10.1126/science.1235773>
- Butnor, J., Roth, B., & Johnsen, K. (2005). *Feasibility of using ground-penetrating radar to quantify root mass in Florida's intensively managed pine plantations* (FBRC Report #38). University of Florida.
- Butnor, J. R., Doolittle, J., Kress, L., Cohen, S., & Johnsen, K. H. (2001). Use of ground-penetrating radar to study tree roots in the southeastern United States. *Tree Physiology*, *21*(17), 1269–1278. <https://doi.org/10.1093/treephys/21.17.1269>

- Chanzy, A., Tarussov, A., Bonn, F., & Judge, A. (1996). Soil water content determination using a digital ground-penetrating radar. *Soil Science Society of America Journal*, 60(5), 1318–1326. <https://doi.org/10.2136/sssaj1996.03615995006000050005x>
- Cheng, N.-F., Tang, H.-W. C., & Ding, X.-L. (2014). A 3d model on tree root system using ground penetrating radar. *Sustainable Environment Research*, 24(4), 291–301.
- Comas, L. H., Anderson, L., Dunst, R., Lakso, A., & Eissenstat, D. (2005). Canopy and environmental control of root dynamics in a long-term study of concord grape. *New Phytologist*, 167(3), 829–840. <https://doi.org/10.1111/j.1469-8137.2005.01456.x>
- Cui, X. H., Chen, J., Shen, J. S., Cao, X., Chen, X. H., & Zhu, X. L. (2011). Modeling tree root diameter and biomass by ground-penetrating radar. *Science China Earth Sciences*, 54, 711–719. <https://doi.org/10.1007/s11430-010-4103-z>
- Daniels, J. J. (2000). *Ground penetrating radar fundamentals*. https://www.researchgate.net/profile/Jeffrey-Daniels/publication/237508286_Ground_Penetrating_Radar_Fundamentals/links/540ed41a0cf2f2b29a3b51a3/Ground-Penetrating-Radar-Fundamentals.pdf
- Danjon, F., & Reubens, B. (2008). Assessing and analyzing 3d architecture of woody root systems, a review of methods and applications in tree and soil stability, resource acquisition and allocation. *Plant and Soil*, 303, 1–34. <https://doi.org/10.1007/s11104-007-9470-7>
- Day, S. D., Wiseman, P. E., Dickinson, S. B., & Harris, J. R. (2010). Contemporary concepts of root system architecture of urban trees. *Arboriculture & Urban Forestry*, 36(4), 149–159.
- de Dorlodot, S., Forster, B., Pagès, L., Price, A., Tuberosa, R., & Draye, X. (2007). Root system architecture: Opportunities and constraints for genetic improvement of crops. *Trends in Plant Science*, 12(10), 474–481. <https://doi.org/10.1016/j.tplants.2007.08.012>
- Dias, A., Gaspar, M. J., Carvalho, A., Pires, J., Lima-Brito, J., Silva, M. E., & Louzada, J. L. (2018). Within-and between-tree variation of wood density components in pinus nigra at six sites in Portugal. *Annals of Forest Science*, 75, 1–19. <https://doi.org/10.1007/s13595-018-0734-6>
- Domke, G. M., Oswalt, S. N., Walters, B. F., & Morin, R. S. (2020). Tree planting has the potential to increase carbon sequestration capacity of forests in the United States. *Proceedings of the National Academy of Sciences*, 117(40), 24649–24651. <https://doi.org/10.1073/pnas.2010840117>
- Drexhage, M., & Colin, F. (2001). Estimating root system biomass from breast-height diameters. *Forestry*, 74(5), 491–497. <https://doi.org/10.1093/forestry/74.5.491>
- esri. (2011). ArcMap 10.0 [Computer software]. Environmental Systems Research Institute. <https://www.esri.com>
- Fan, G., Liang, H., Zhao, Y., & Li, Y. (2022). Automatic reconstruction of three-dimensional root system architecture based on ground-penetrating radar. *Computers and Electronics in Agriculture*, 197, 106969.
- Gašparíková, O., Mistrík, I., & Čiamporová, M. (2002). Waisel, Y., Eshel, A., Kafkafi, U., eds. Plant roots-the hidden half. *Annals of Botany*, 90(6), 775–776. <https://doi.org/10.1093/aob/mcf252>
- Guideline Geo. (2023). MALA vision software: GPR Data Acquisition and Processing Manual. (Version 3.0) [Computer software]. Guideline Geo. <https://www.guidelinegeo.com>
- Guo, L., Chen, J., Cui, X., Fan, B., & Lin, H. (2013). Application of ground-penetrating radar for coarse root detection and quantification: A review. *Plant and Soil*, 362, 1–23. <https://doi.org/10.1007/s11104-012-1455-5>
- Hansen, S. M., Maughan, T., Barlow, B., & Black, B. (2018). *Tart cherries in the garden*. <https://digitalcommons.usu.edu/cgi/viewcontent.cgi?article=2917&context=extension%5Fcurreall>
- Hodge, A. (2004). The plastic plant: Root responses to heterogeneous supplies of nutrients. *New Phytologist*, 162, 9–24. <https://doi.org/10.1111/j.1469-8137.2004.01015.x>
- Hruska, J., Cerma'k, J., & Sustek, S. (1999). Mapping tree root systems with ground-penetrating radar. *Tree Physiology*, 19, 125–130. <https://doi.org/10.1093/treephys/19.2.125>
- Hwang, S.-W., & Sugiyama, J. (2021). Computer vision-based wood identification and its expansion and contribution potentials in wood science: A review. *Plant Methods*, 17(1), 1–21. <https://doi.org/10.1186/s13007-021-00746-1>
- Jackson, R. B., Mooney, H. A., & Schulze, E. D. (1997). A global budget for fine root biomass, surface area, and nutrient contents. *Proceedings of the National Academy of Sciences*, 94(14), 7362–7366.
- Jol, H. M. (1995). Ground-penetrating radar antennae frequencies and transmitter powers compared for penetration depth, resolution and reflection continuity1. *Geophysical Prospecting*, 43(5), 693–709. <https://doi.org/10.1111/j.1365-2478.1995.tb00275.x>
- Jol, H. M. (Ed.). (2008). *Ground-penetrating radar theory and applications*. Elsevier.
- Kimberley, M. O., Cown, D. J., McKinley, R. B., Moore, J. R., & Dowling, L. J. (2015). Modelling variation in wood density within and among trees in stands of New Zealand-grown radiata pine. *New Zealand Journal of Forestry Science*, 45, 1–13. <https://doi.org/10.1186/s40490-015-0053-8>
- Kurz, W., Dymond, C., White, T., Stinson, G., Shaw, C., Rampley, G., Smyth, C., Simpson, B., Neilson, E., Trofymow, J., Metsaranta, J., & Apps, M. J. (2009). Cbm-cfs3: A model of carbon-dynamics in forestry and land-use change implementing IPCC standards. *Ecological Modelling*, 220(4), 480–504. <https://doi.org/10.1016/j.ecolmodel.2008.10.018>
- Lamlom, S. H., & Savidge, R. A. (2006). Carbon content variation in boles of mature sugar maple and giant sequoia. *Tree Physiology*, 26(4), 459–468. <https://doi.org/10.1093/treephys/26.4.459>
- Lantini, L., Giannakis, I., Tosti, F., Mortimer, D., & Alani, A. M. (2020a). A reflectivity-based GPR signal processing methodology for mapping tree root systems of street trees. In *2020 43rd International Conference on Telecommunications and Signal Processing (TSP)* (pp. 449–452). IEEE. <https://doi.org/10.1109/TSP49548.2020.9163517>
- Lantini, L., Tosti, F., Giannakis, I., Zou, L., Benedetto, A., & Alani, A. M. (2020b). An enhanced data processing framework for mapping tree root systems using ground-penetrating radar. *Remote Sensing*, 12, 1–33. <https://doi.org/10.3390/rs12203417>
- Li, S., Brandt, M., Fensholt, R., Kariryaa, A., Igel, C., Gieseke, F., Nord-Larsen, T., Oehmcke, S., Carlsen, A. H., Juntila, S., Tong, X., d'Aspremont, A., & Ciais, P. (2023). Deep learning enables image-based tree counting, crown segmentation, and height prediction at national scale. *PNAS Nexus*, 2(4), pgad076. <https://doi.org/10.1093/pnasnexus/pgad076>
- Li, X., Ingvorsen, C. H., Weiss, M., Rebetzke, G. J., Condon, A. G., James, R. A., & Richards, R. A. (2019). Deeper roots associated with cooler canopies, higher normalized difference vegetation index, and greater yield in three wheat populations grown on stored soil water. *Journal of Experimental Botany*, 70(18), 4963–4974. <https://doi.org/10.1093/jxb/erz232>

- Lorenz, K., & Lal, R. (2014). Soil organic carbon sequestration in agroforestry systems. A review. *Agronomy for Sustainable Development*, 34, 443–454. <https://doi.org/10.1007/s13593-014-0212-y>
- Lunt, I., Hubbard, S., & Rubin, Y. (2005). Soil moisture content estimation using ground-penetrating radar reflection data. *Journal of Hydrology*, 307(1–4), 254–269. <https://doi.org/10.1016/j.jhydrol.2004.10.014>
- Lynch, J. (1995). Root architecture and plant productivity. *Plant Physiology*, 109(1), 7–13. <https://doi.org/10.1104/pp.109.1.7>
- Lynch, J. P. (2007). Roots of the second green revolution. *Australian Journal of Botany*, 55, 493–512. <https://doi.org/10.1071/BT06118>
- MacFarlane, D. W. (2020). Functional relationships between branch and stem wood density for temperate tree species in north America. *Frontiers in Forests and Global Change*, 3, 63. <https://doi.org/10.3389/ffgc.2020.00063>
- McCarthy, H. R., Pataki, D. E., & Jenerette, G. D. (2011). Plant water-use efficiency as a metric of urban ecosystem services. *Ecological Applications*, 21, 3115–3127. <https://doi.org/10.1890/11-0048.1>
- Me-Nsope, N. M. (2009). *Tart cherry yield and economic response to alternative planting densities* [Master's thesis, Michigan State University].
- Mildrexler, D. J., Berner, L. T., Law, B. E., Birdsey, R. A., & Moomaw, W. R. (2020). Large trees dominate carbon storage in forests east of the cascade crest in the united states pacific northwest. *Frontiers in Forests and Global Change*, 3, 594274.
- Millard, S., Shaari, A., & Bungey, J. (2002). Field pattern characteristics of GPR antennas. *NDT & E International*, 35(7), 473–482.
- Mokany, K., Raison, R. J., & Prokushkin, A. S. (2006). Critical analysis of root: Shoot ratios in terrestrial biomes. *Global Change Biology*, 12(1), 84–96. <https://doi.org/10.1111/j.1365-2486.2005.001043.x>
- Molon, M., Boyce, J. I., & Arain, M. A. (2017). Quantitative, nondestructive estimates of coarse root biomass in a temperate pine forest using 3-d ground-penetrating radar (GPR). *Journal of Geophysical Research: Biogeosciences*, 122(1), 80–102. <https://doi.org/10.1002/2016JG003518>
- Morhart, C., Sheppard, J. P., Schuler, J. K., & Spiecker, H. (2016). Aboveground woody biomass allocation and within tree carbon and nutrient distribution of wild cherry (*Prunus avium* L.)—A case study. *Forest Ecosystems*, 3, Article 4. <https://doi.org/10.1186/s40663-016-0063-x>
- Oelbermann, M., Voroney, R. P., & Gordon, A. M. (2004). Carbon sequestration in tropical and temperate agroforestry systems: A review with examples from costa Rica and southern canada. *Agriculture, Ecosystems & Environment*, 104(3), 359–377.
- Ohler, A. (2023). *The best cherry tree varieties to grow in Michigan*. <https://brightlanegardens.com/best-cherry-trees-grow-michigan/>
- Okazaki, H., Nakazato, H., & Kwak, Y. (2013). Application of high-frequency ground penetrating radar to the reconstruction of 3d sedimentary architecture in a flume model of a fluvial system. *Sedimentary Geology*, 293, 21–29. <https://doi.org/10.1016/j.sedgeo.2013.04.001>
- Pallardy, S. G. (2008). The woody plant body. In S. G. Pallardy (Ed.), *Physiology of woody plant* (3rd ed., pp. 9–38). Academic Press.
- Pedregosa, F., Varoquaux, G., Gramfort, A., Michel, V., Thirion, B., Grisel, O., Blondel, M., Prettenhofer, P., Weiss, R., Dubourg, V., Vanderplas, J., Passos, A., Cournapeau, D., Brucher, M., Perrot, M., & Duchesnay, É. (2011). Scikit-learn: Machine learning in Python. *Journal of Machine Learning Research*, 12, 2825–2830.
- Pregitzer, K. S. (2002). Fine roots of trees: A new perspective. *The New Phytologist*, 154(2), 267–270. https://doi.org/10.1046/j.1469-8137.2002.00413_1.x
- Pretzsch, H. (2009). *Forest dynamics, growth, and yield*. Springer. <https://doi.org/10.1007/978-3-540-88307-4>
- Raven, P. H., Evert, R. F., & Eichhorn, S. E. (2005). *Biology of plants*. Macmillan Publishers Ltd.
- Richardson, A. D., & Zu Dohna, H. (2003). Predicting root biomass from branching patterns of Douglas-fir root systems. *Oikos*, 100(1), 96–104. <https://doi.org/10.1034/j.1600-0706.2003.12081.x>
- Salako, J. O. (2023). *Assessing roots distribution of tart cherry tree using ground-penetrating radar (GPR) and artificial intelligence* [Master's thesis, Michigan State University].
- Sandmeier, K. J. (2022). ReflexW: Processing and Interpretation of Reflection Seismic, Refraction Seismic, and GPR Data (Version 9.5) [Computer software]. Sandmeier Geophysical Research Software. <https://www.sandmeier-geo.de/reflexw.html>
- Schneider, C. A., Rasband, W. S., & Eliceiri, K. W. (2012). NIH Image to ImageJ: 25 years of image analysis. *Nature Methods*, 9(7), 671–675. <https://doi.org/10.1038/nmeth.2089>
- Schneider, P., & Xhafa, F. (2022). *Anomaly detection and complex event processing over IoT data streams: With application to EHealth and patient data monitoring*. Academic Press.
- Simonyan, K., & Zisserman, A. (2014). Very deep convolutional networks for large-scale image recognition. arXiv. <https://doi.org/10.48550/arXiv.1409.1556>
- Sinacore, K., Hall, J. S., Potvin, C., Royo, A. A., Ducey, M. J., & Ashton, M. S. (2017). Unearthing the hidden world of roots: Root biomass and architecture differ among species within the same guild. *PLOS One*, 12(10), e0185934. <https://doi.org/10.1371/journal.pone.0185934>
- Sirrine, J., Letourneau, D., Shennan, C., Sirrine, D., Fouch, R., Jackson, L., & Mages, A. (2008). Impacts of groundcover management systems on yield, leaf nutrients, weeds, and arthropods of tart cherry in Michigan, USA. *Agriculture, Ecosystems & Environment*, 125(1–4), 239–245.
- Smith, S., & De Smet, I. (2012). Root system architecture: Insights from *Arabidopsis* and cereal crops. *Philosophical Transactions of the Royal Society of London. Series B, Biological Sciences*, 367(1595), 1441–1452. <https://doi.org/10.1098/rstb.2011.0234>
- Sordo, Z., Andeer, P., Sethian, J., Northen, T., & Ushizima, D. (2024). Rhizonet segments plant roots to assess biomass and growth for enabling self-driving labs. *Scientific Reports*, 14(1), 12907. <https://doi.org/10.1038/s41598-024-63497-8>
- Sun, D., Jiang, F., Wu, H., Liu, S., Luo, P., & Zhao, Z. (2023). Root location and root diameter estimation of trees based on deep learning and ground-penetrating radar. *Agronomy*, 13(2), 344. <https://doi.org/10.3390/agronomy13020344>
- Tosti, F., Patriarca, C., Slob, E., Benedetto, A., & Lambot, S. (2013). Clay content evaluation in soils through GPR signal processing. *Journal of Applied Geophysics*, 97, 69–80. <https://doi.org/10.1016/j.jappgeo.2013.04.006>
- Tracy, S. R., Black, C. R., Roberts, J. A., & Mooney, S. J. (2011). Soil compaction: A review of past and present techniques for investigating effects on root growth. *Journal of the Science of Food and Agriculture*, 91(9), 1528–1537. <https://doi.org/10.1002/jsfa.4424>
- Tumber-D'avila, S. J., Schenk, H. J., Du, E., & Jackson, R. B. (2022). Plant sizes and shapes above and belowground and their interactions with climate. *New Phytologist*, 235(3), 1032–1056. <https://doi.org/10.1111/nph.18031>

- van Noordwijk, M., Cadisch, G., & Ong, C. K. (Eds.). (2004). *Below-ground interactions in tropical agroecosystems: Concepts and models with multiple plant components*. CABI.
- Vignati, E., Lipska, M., Dunwell, J. M., Caccamo, M., & Simkin, A. J. (2022). Fruit development in sweet cherry. *Plants*, 11(12), 1531. <https://doi.org/10.3390/plants11121531>
- Virtanen, P., Gommers, R., Oliphant, T. E., Haberland, M., Reddy, T., Cournapeau, D., Burovski, E., Peterson, P., Weckesser, W., Bright, J., van der Walt, S. J., Brett, M., Wilson, J., Millman, K. J., Mayorov, N., Nelson, A. R. J., Jones, E., Kern, R., Larson, E., ... Van Mulbregt, P. (2020). SciPy 1.0: Fundamental algorithms for scientific computing in Python. *Nature Methods*, 17(3), 261–272. <https://doi.org/10.1038/s41592-019-0686-2>
- Weihs, B. J., Heuschele, D.-J., Tang, Z., York, L. M., Zhang, Z., & Xu, Z. (2024). The state of the art in root system architecture image analysis using artificial intelligence: A review. *Plant Phenomics*, 6, 0178. <https://doi.org/10.34133/plantphenomics.0178>
- Wielopolski, L., Hendrey, G., Daniels, J., & McGuigan, M. (2000). Imaging tree root systems in situ. In *Eighth International Conference on Ground Penetrating Radar* (Vol. 4084, pp. 642–646). SPIE.
- Zajícová, K., & Chuman, T. (2019). Application of ground-penetrating radar methods in soil studies: A review. *Geoderma*, 343, 116–129. <https://doi.org/10.1016/j.geoderma.2019.02.024>
- Zhang, X., Derival, M., Albrecht, U., & Ampatzidis, Y. (2019). Evaluation of a ground-penetrating radar to map the root architecture of HLB-infected citrus trees. *Agronomy*, 9, 354. <https://doi.org/10.3390/agronomy9070354>
- Zhang, X., & Wang, W. (2015). The decomposition of fine and coarse roots: Their global patterns and controlling factors. *Scientific Reports*, 5(1), 9940. <https://doi.org/10.1038/srep09940>
- Zhu, S., Huang, C., Su, Y., & Sato, M. (2014). 3d ground-penetrating radar to detect tree roots and estimate root biomass in the field. *Remote Sensing*, 6, 5754–5773. <https://doi.org/10.3390/rs6065754>

SUPPORTING INFORMATION

Additional supporting information can be found online in the Supporting Information section at the end of this article.

How to cite this article: Salako, J., Millar, N., Kendall, A., & Basso, B. (2025). Assessing tree root distributions using ground-penetrating radar and machine learning algorithms. *Agrosystems, Geosciences & Environment*, 8, e70217. <https://doi.org/10.1002/agg2.70217>